applied sciences

MDPI

Article

Optimal Sizing and Placement of Reactive Power Compensation in Rural Distribution Networks Using an Experience Exchange Strategy

Juan M. Lujano-Rojas, Rodolfo Dufo-López *, Jesús S. Artal-Sevil and José L. Bernal-Agustín

Department of Electrical Engineering, University of Zaragoza, Calle María de Luna 3, 50018 Zaragoza, Spain; lujano.juan@unizar.es (J.M.L.-R.); jsartal@unizar.es (J.S.A.-S.); jlbernal@unizar.es (J.L.B.-A.)
* Correspondence: rdufo@unizar.es

Abstract

Reactive power compensation devices (RPCDs) are crucial for improving the efficiency of energy systems. Distribution systems are commonly modeled under the simplifying assumption of balanced operation, which does not accurately represent real operating conditions. Motivated by the need to develop an effective computational tool for the proper selection of RPCDs, this paper proposes the application of the experience exchange strategy (EES) to the coordinated design of RPCDs. To the best of the authors' knowledge, this is the first study to employ EES for this purpose. The proposed methodology is validated through two case studies. In the first case, an extensive exploration of the search space is performed by repeating the optimization process, resulting in a solution with a high probability of being the global optimum. Under this scenario, a comparative analysis shows that EES outperforms the genetic algorithm by 7.4%. In the second case, EES is compared with other popular heuristic techniques, including particle swarm optimization (PSO), without performing a deep exploration of the search space, observing that EES ranks in the middle, with a difference of 11.9% relative to PSO. Overall, the results confirm that the proposed EES-based framework constitutes a reliable and efficient approach.

Keywords: experience exchange strategy; genetic algorithm; heuristic optimization; rural distribution systems; reactive power compensation

1. Introduction

The growth in electricity demand, closely associated with societal and technological development, can increase the operational complexity of transmission and distribution systems (DSs), driving them toward operation near their limits and potentially leading to system-wide instability or collapse. In this context, reactive power compensation devices (RPCDs) can enhance power transfer capability, improve system stability and efficiency, and reduce congestion, power losses, and operating costs [1].

Determining the optimal size and location of RPCDs requires the analysis of multiple techno-economic factors, making it a labor-intensive problem. Under these circumstances, optimization techniques are commonly employed to obtain cost-effective designs [1].

The optimization methods commonly employed for the sizing and placement of RPCDs can be classified into analytical approaches, traditional (or conventional) techniques, metaheuristic algorithms, and hybrid methodologies that combine analytical and metaheuristic approaches. In brief, analytical approaches are computationally simple and

Academic Editor: Alexander Barkalov

Received: 23 February 2026
Revised: 16 March 2026
Accepted: 18 March 2026
Published: 20 March 2026

efficient; however, they often fail to capture the nonlinear and complex characteristics of electrical systems. Traditional techniques refer to well-established optimization methods such as linear programming, nonlinear programming, dynamic programming, and sequential quadratic programming, among others. Metaheuristic algorithms are typically inspired by natural processes, which are abstracted to guide the search toward a specific objective and an effective solution strategy. These algorithms can be further categorized according to their source of inspiration, including biology-, physics-, and chemistry-inspired methods. Hybrid analytical–metaheuristic approaches are adopted to achieve improved solutions by exploiting the complementary advantages of each methodology [1].

A representative case illustrating the benefits of adopting RPCDs is the operational analysis of the Urmia Petrochemical Plant [2], for which the reported results are promising in terms of electrical efficiency and power quality. When improvements in voltage profile and power factor are considered the primary objectives for enhancing overall system performance, compensating reactive power at the main buses—namely, along the primary delivery feeder—yields the most favorable outcomes. In the specific case of the Urmia Petrochemical Plant, improvements in electrical system efficiency enable a reduction of approximately 1.3% in power imports from the bulk power system.

Asabere et al. [3] implemented a methodology for the optimal dimensioning and placement of distribution static compensators using particle swarm optimization (PSO) to reduce system losses and improve the voltage profile. The authors demonstrated the effectiveness of their approach through a case study of a distribution network located in the Ashanti Region of Ghana, where economic activity is primarily driven by mining, agriculture, and manufacturing. According to the reported results, optimal reactive power compensation achieved via PSO leads to a 16.3% improvement in the voltage profile, along with a significant increase in overall system efficiency.

Rajak et al. [4] developed and implemented two methodologies for the sizing and placement of RPCDs, using the voltage deviation index as the primary objective function. In the first methodology, the candidate buses for RPCD installation are identified through sequential load sensitivity analysis, while the optimal device sizes are determined using a hybrid approach that combines the student psychology-based optimization (SPBO) algorithm with particle swarm optimization (PSO). In the second methodology, the authors also employed a combined SPBO–PSO framework, but formulated it as a mixed discrete optimization model. Based on the case-study analysis, the authors reported that the second approach achieved superior performance from both economic and environmental perspectives.

Adegoke [5] enhanced the PSO algorithm by incorporating a cosine-based inertia weight and applied it to the problem of sizing and placement of RPCDs, with the objectives of minimizing power losses, improving the voltage profile, and enhancing DS reliability. Based on several computational experiments conducted on the IEEE 33-bus and 39-bus distribution systems, the author reported encouraging results in terms of reduced energy losses and deferred infrastructure upgrades. Moreover, the effectiveness of the proposed inertia-weight formulation was validated using the Wilcoxon rank-sum and Friedman tests, suggesting that the improved PSO algorithm could be extended to address a broader range of engineering optimization problems.

Amekah et al. [6] developed a technique for the sizing and placement of RPCDs based on a combination of dynamic programming (DP) and the conditional new adaptive foraging tree squirrel search algorithm (CNAFTSSA). The authors aimed to minimize power losses while improving power quality. Moreover, the proposed approach demonstrated promising results when compared with PSO and the genetic algorithm (GA).

Jahed et al. [7] developed an approach for the sizing and placement of RPCDs based on the water flow optimization (WFO) algorithm. The proposed technique aims to reduce power losses and the costs associated with the required equipment, while improving the voltage profile. The authors conducted a comparative study on the IEEE-33-bus and IEEE-69-bus test systems against other well-established optimization techniques, including PSO and GA, and reported favorable results.

With a particular focus on the bulk power system, Bhattacharyya et al. [8] developed a model for the optimal dimensioning of RPCDs—specifically unified power flow controllers (UPFCs), thyristor-controlled series compensators (TCSCs), and static VAr compensators—with the objective of minimizing total operating costs. The authors performed a power flow analysis to identify candidate buses for RPCD installation by examining reactive power flows. To address the associated optimization problem, they employed the sine cosine algorithm (SCA), achieving a cost reduction of approximately 28.06% on the IEEE-57 test system. Moreover, the authors used the Wilcoxon signed-rank test to compare SCA with several other optimization techniques, including PSO, and concluded that SCA exhibits excellent performance. To address the problem of RPCD placement, the authors in [9] implemented several techniques, including modal analysis, loss-sensitivity analysis, the line stability index, and the fast voltage stability index, to determine the appropriate installation buses. Consequently, the proposed framework for the optimal dimensioning and placement of RPCDs is comprehensive.

Gómez et al. [10] presented a method based on the basin-hopping algorithm (BHA) combined with an adaptive search-space reduction strategy, which reduces the complexity of the optimization problem while preserving solution quality. Unlike other techniques reported in the literature, the proposed optimization framework aims to minimize the total short-circuit contributions of the connected RPCDs, which are assumed to be synchronous condensers and inverter-based resources. This perspective enables decision makers to avoid overestimating the required size of compensation equipment, thereby enhancing system reliability, particularly in weak grids.

Singh and Kumar [11] proposed an RPCD sizing approach capable of determining the optimal locations of electric vehicle charging stations, thereby enabling decision makers to mitigate the impact of electric transportation on power quality. The methodology performs the optimal dispatch of active and reactive power by solving the associated optimal power flow (OPF) problem using a local randomized neural network (LRNN). The optimization problem is formulated to minimize power losses and associated costs and enhance system reliability. Through the analysis of a representative case study, the authors compared their approach with other methods, including GA and PSO, and reported high-quality solutions with low computational times.

Ebeed et al. [12] developed a model to address the OPF problem, emphasizing the role of reactive power and its management through the optimal setting of UPFCs. The authors incorporate sources of uncertainty related to renewable power generation and medium-term load demand growth, thereby transforming the optimization problem into a stochastic one. This problem is addressed using the adaptive beluga whale optimization (ABWO) algorithm, which was subsequently tested on the IEEE-30 test system, yielding a reduction in power losses of approximately 25% and a voltage deviation reduction of about 40%.

Alnami [13] proposed a placement technique based on the electric eel foraging optimizer (EEFO) to minimize power losses and enhance the overall voltage profile. To reduce computational complexity, the author introduced two strategies depending on whether the compensation capacitors are treated as decision variables. The effectiveness of EEFO was

demonstrated through an analysis of the IEEE-33-bus system and comparisons with PSO and GA.

Mathenge et al. [14] developed a sizing and placement model based on solving the OPF problem using the crow search algorithm (CSA), with the objective of minimizing operating costs while improving the voltage profile. An analysis of the IEEE-33-bus test system demonstrated the superior performance of CSA compared with other optimization techniques, including GA and PSO.

Sharma and Ghosh [15] proposed a comprehensive planning model for DSs. On one hand, the planning problem is formulated by considering power losses, short-circuit capacity, and energy not supplied, and is solved using PSO. On the other hand, the sizing of RPCDs is performed under multiple load levels using a hybrid artificial bee colony–cuckoo search optimization (ABC–CSO) algorithm. Consequently, the proposed framework provides an accurate long-term solution by incorporating relevant planning information.

Badrudeen et al. [16] analyzed the placement and sizing of RPCDs commonly employed in transmission systems, including the static synchronous compensator (STATCOM). To this end, the authors evaluated the maximum reactive power loadability using a novel voltage stability index. Subsequently, the optimal sizing procedure was carried out using the firefly algorithm (FA) combined with the dingo optimization algorithm (DOA). Key aspects related to power losses in transmission lines and voltage profile were examined through case studies on the IEEE-33-bus and IEEE-57-bus systems, resulting in power loss reductions of 14.18% and 19.95%, respectively.

Patiño et al. [17] proposed a design model for the optimal sizing and placement of RPCDs, including the distribution of STATCOMs, based on a mixed-integer linear programming (MILP) approach capable of incorporating daily system behavior. Through the analysis of distribution systems with 33, 69, and 136 buses, the authors observed power loss reductions of up to 23%, accompanied by economic profitability improvements of up to 15%.

Patel et al. [18] proposed a methodology for the optimal placement of RPCDs, including distribution STATCOMs and TCSCs, in which the blue whale optimization (BWO) algorithm is combined with the salp swarm algorithm (SSA), while accounting for uncertainties related to renewable resources. In addition, the real-time control strategy is enhanced by incorporating a proportional–integral–derivative scheme, thereby improving voltage stability. Regarding the optimization objectives, the proposed technique considers power loss reduction, voltage stability enhancement, and operating costs. An analysis of a representative case study revealed reductions of 42.1% in power losses and 46.85% in voltage violations, demonstrating the capability of the approach to enhance DS performance.

Okendo and Farzaneh [19] introduced a design model for RPCDs formulated as a multi-objective mixed-integer nonlinear programming (MINLP) problem capable of accounting for the power losses of energy conversion devices associated with renewable power generation. The primary objectives of the optimization process are the cost of energy and voltage stability. Through the analysis of a representative case study, the authors demonstrated the significance of power losses in renewable energy components, which ranged between 13.32% and 24.46%, and their impact on the optimization outcomes.

Das et al. [20] introduced a solution to the OPF problem for a high-voltage AC–DC transmission system, using the JAYA algorithm to minimize power losses while improving system voltage profiles. Through the analysis of several IEEE test power systems, the authors observed power loss reductions ranging from 20.71% to 59.17%, depending on system size and structure.

Fotis [21] developed a planning model capable of incorporating the effects of electric transportation system charging stations into the electrical network. The methodology is based on the binary random dynamic arithmetic optimization algorithm (BRDAOA), which is implemented to address power losses, total harmonic distortion, and total voltage deviation, subject to the system's operational constraints.

Table 1 summarizes key information from the aforementioned studies. As can be observed, most of the employed techniques are essentially heuristic and yield satisfactory results. However, the DS is frequently modeled under the basic assumption of balanced operation, which is not an intrinsic characteristic at the distribution level.

Table 1. Brief description of recently proposed algorithms for RPCD sizing and placement.

Paper	Algorithm	Methodology
[3]	PSO	The methodology is capable of incorporating advanced equipment for reactive power compensation. Nevertheless, the employed power flow routine fails to capture the unbalanced behavior of conventional distribution networks. Regarding reactive power injection, it is not obtained from a power flow analysis but rather approximated using a simplified circuit expression, which reduces the accuracy of the results.
[4]	Mixed discrete SPBO–PSO	The mixed discrete SPBO–PSO model demonstrated its effectiveness in terms of annual profit and emission reduction associated with distributed generation. However, the simulation framework does not account for the unbalanced operation of the distribution network. The reactive power to be provided by the RPCD is determined using an expression that depends linearly on the reactive power load demand, without considering the voltage at the connection point. In other words, the relationship between the bus voltage and the reactive power supplied by the RPCD is not mathematically represented.
[5]	Improved PSO	The authors enhanced the PSO algorithm and employed the Wilcoxon rank-sum and Friedman tests to demonstrate its effectiveness relative to other optimization techniques. Nevertheless, the simulation framework does not consider the unbalanced operating conditions of the distribution network. The reactive power to be injected by an RPCD is limited by the reactive power demand of the load at the corresponding connection bus. Thus, the method only compensates for the load's reactive power and is not capable of increasing the voltage to a predefined value.
[6]	DP and CNAFTSSA	The study analyzes various operating conditions of load demand and renewable generation, as well as the impact of reactive power injection using CNAFTSSA, thereby providing a comprehensive perspective on improving DS performance. Nevertheless, the implemented power flow routine does not account for the unbalanced nature of typical distribution systems. The RPCD is represented using a basic capacitor model without any control circuit, which does not allow us to account for its effect on the voltage at the connection bus.
[7]	WFO	The authors proposed a model based on reactive power tariffs, which are subsequently employed by the WFO algorithm for the optimal sizing and placement tasks. Nevertheless, the adopted simulation framework neglects the unbalanced operating characteristics of the distribution network. The reactive power from the RPCDs is assigned to improve the load power factor at the connection bus, without considering any setting related to the corresponding voltage.
[8,9]	SCA	The authors developed a dimensioning model primarily intended for transmission systems, which are typically electrically balanced. However, the RPCD placement method relies solely on power flow analysis, which may result in designs with uncertain economic profitability. To address this issue, the authors propose the use of the line stability index. The method essentially relies on several indices to identify weak nodes, which then determine the placement of the RPCDs. Subsequently, the reactive power injection is calculated using a heuristic optimization method. This procedure is computationally light, but it reduces the accuracy of the stage related to RPCD placement.

Table 1. *Cont.*

Paper	Algorithm	Methodology
[10]	BHA	The authors incorporate relevant technical aspects, such as grid strength. However, no economic index is included in the optimization process. The optimization process does not involve any economic parameters. It is essentially a technical analysis aimed at improving system performance in terms of grid strength.
[11]	LRNN	This approach incorporates the effects of electric transportation on DSs. Nevertheless, specific characteristics of DSs, such as their unbalanced nature, are not taken into account. The reactive power is not adjusted to achieve a specified voltage at the connection bus. Instead, it is determined based on the reactive power balance principle.
[12]	ABWO	The proposed sizing model is primarily applicable to transmission systems, which typically operate under balanced electrical conditions. The methodology is not intended to determine the optimal placement of RPCDs; it only optimizes reactive power dispatch.
[13]	EEFO	The proposed methodology reduces the computational complexity of the optimization problem. Nevertheless, the employed simulation framework overlooks the inherently unbalanced nature of distribution network operation. The authors evaluate the effects of reactive power by considering up to four devices. In other words, the methodology is not formulated to maximize system performance in a general sense.
[14]	CSA	The authors proposed an effective model able to find a robust and economically attractive solution. However, the employed power flow routine is unable to adequately represent the unbalanced behavior of typical distribution networks. The optimization model does not incorporate the impact of reactive power injection at the connection bus. In fact, the model limits the total reactive power to the value demanded by the loads.
[15]	PSO and ABC-CSO	The authors developed a comprehensive framework for addressing the expansion problem of DSs. Nevertheless, the employed power flow routine is incapable of accurately representing the unbalanced operating conditions commonly observed in distribution networks. The placement methodology is based on a sensitivity index related to voltage collapse, which could lead to suboptimal designs.
[16]	FA-DOA	The proposed sizing framework is chiefly applicable to transmission systems, which are characteristically electrically balanced. The placement of RPCDs is carried out using a maximum loadability index rather than a combinatorial analysis, which could lead to suboptimal configurations.
[17]	MILP	The use of MILP provides system designers with optimal solutions within the context of a linearized mathematical model. However, the estimation of reactive power effects may be inaccurate, as the nonlinear power flow equations are not explicitly solved.
[18]	BWO-SSA	The methodology is capable of improving voltage stability in a cost-effective manner. Nonetheless, the adopted power flow formulation is insufficient to accurately represent the inherently unbalanced behavior of conventional distribution networks. The placement methodology is based on the analysis of the eigenvalues of the Jacobian matrix, which may lead to suboptimal results due to the lack of a combinatorial approach.
[19]	Multi-objective MINLP	The methodology incorporates relevant aspects related to the estimation of system efficiency. Nonetheless, the power flow routine used lacks the capability to properly model the unbalanced characteristics of practical distribution networks. The technique employs a voltage stability index, which reduces the computational burden but also decreases the precision of the obtained results due to the lack of a combinatorial analysis of the candidate buses.
[20]	JAYA	The proposed sizing framework is chiefly applicable to transmission systems, which are characteristically electrically balanced.
[21]	BRDAOA	The research does not account for the specific characteristics of distribution networks related to unbalanced operation. On the other hand, it is based on the estimation of the loss sensitivity factor to determine the optimal placement, which could lead to near-optimal solutions.

Under these conditions and motivated by the need to develop an effective computational tool for the proper selection of RPCDs, the main contributions of this research are as follows:

- Incorporating the unbalanced operation of the DS into the optimization process for the sizing and placement of RPCDs enables per-phase specification of device capacities, thereby allowing a more accurate assessment of their impact on the voltage profile.
- Implementing the experience exchange strategy (EES) for the design of RPCDs. To the best of our knowledge, this is the first time that this algorithm has been applied in this field, offering a computationally efficient means of obtaining high-quality solutions from a techno-economic perspective.
- Sensitivity factors are typically formulated assuming a balanced power system. However, distribution networks are intrinsically unbalanced, which makes the application of sensitivity factors more difficult. Since the proposed model in this paper implements the interaction between the dispatch and placement of RPCDs in a nested manner, it is not necessary to employ sensitivity factors, which enhances the quality of the results. This represents a notable difference from many planning techniques previously published.

The remainder of the paper is organized as follows: Section 2 describes the structure of the considered DSs; Section 3 explains the implementation of the EES for the optimal sizing and placement of RPCDs; Section 4 illustrates the proposed method through two representative examples; and Section 5 presents the main conclusions and remarks.

2. Model of the Basic Distribution System

Rural electrical systems, such as those typically found in rural areas, are composed of overhead distribution lines arranged in a radial configuration. The impedance of each line can be modeled based on its physical structure. Accordingly, for a system operating at 60 Hz, the positive- and negative-sequence impedances of the overhead lines can be estimated using Equation (1) [22]:

$$Z^{+}_{(m)} = Z^{-}_{(m)} = R^{phase}_{(m)} + \left(\sqrt{-1}\right)\left\{0.0529 \times log_{10}\left(\frac{GMD^{phase}_{(m)}}{GMR^{phase}_{(m)}}\right)\right\}, \quad (1)$$

where $Z^{+}_{(m)}$ and $Z^{-}_{(m)}$ denote the positive- and negative-sequence impedances, respectively; $R^{phase}_{(m)}$ is the resistance of the phase conductor (Ω/1000 ft); and $GMD^{phase}_{(m)}$ and $GMR^{phase}_{(m)}$ represent the geometric mean distance and geometric mean radius of the phase conductor of line m ($m = 1, \ldots, M$), respectively.

Regarding the estimation of the zero-sequence impedances, these depend on the earth return path and its influence on the circuit. In this study, a simplified form of Carson's equations is employed, in which terms dependent on conductor height, end effects, and leakage currents are neglected. In addition, the adopted model assumes that the multigrounded neutral is perfectly coupled to the earth, that all phase conductors have identical dimensions, and that the ground is infinite and has uniform resistivity. The zero-sequence impedance ($Z^{0}_{(m)}$) of a three-wire line is given by Equation (2) [22]:

$$\begin{aligned} Z^{0}_{(m)} = \{R^{phase}_{(m)} \quad & +0.0542\} \\ & +\sqrt{-1}\left\{0.1587 \times log_{10}\left(\frac{278.9\sqrt{\rho_{earth}}}{\sqrt[3]{GMR^{phase}_{(m)}\left(GMD^{phase}_{(m)}\right)^{2}}}\right)\right\} \end{aligned} \quad (2)$$

where ρ_{earth} is the earth resistivity (Ωm). The zero-sequence impedance of a four-wire multigrounded system is given by Equation (3) [22]:

$$Z^0_{(m)} = \{R^{phase}_{(m)} + 0.0542\} + \sqrt{-1}\left\{0.1587 \times log_{10}\left(\frac{278.9\sqrt{\rho_{earth}}}{\sqrt[3]{GMR^{phase}_{(m)}\left(GMD^{phase}_{(m)}\right)^2}}\right)\right\} - 3\left(\frac{Z^{mutual}_{neutral(m)}{}^2}{Z^{self}_{neutral(m)}}\right) \quad (3)$$

where $Z^{self}_{neutral(m)}$ is the self-impedance of the neutral conductor taking account of the earth return, while $Z^{mutual}_{neutral(m)}$ is the mutual impedance between the phase conductors considered as a group and the neutral conductor. The impedances $Z^{self}_{neutral(m)}$ and $Z^{mutual}_{neutral(m)}$ are calculated using Equations (4) and (5) [22]:

$$Z^{self}_{neutral(m)} = \left\{R^{neutral}_{(m)} + 0.01807\right\} + \sqrt{-1}\left\{0.0529 \times log_{10}\left(\frac{278.9\sqrt{\rho_{earth}}}{GMR^{neutral}_{(m)}}\right)\right\}, \quad (4)$$

$$Z^{mutual}_{neutral(m)} = 0.01807 + \sqrt{-1}\left\{0.0529 \times log_{10}\left(\frac{278.9\sqrt{\rho_{earth}}}{GMD^{neutral}_{(m)}}\right)\right\}, \quad (5)$$

where $GMD^{neutral}_{(m)}$ and $GMR^{neutral}_{(m)}$ represent the geometric mean distance and geometric mean radius of the neutral conductor of line m ($m = 1, \ldots, M$), respectively. The zero-sequence impedance of a four-wire unigrounded system is given by Equation (6) [22]:

$$Z^0_{(m)} = R^{phase}_{(m)} + 3R^{neutral}_{(m)} + \sqrt{-1}\left\{R^{neutral}_{(m)} + 0.1587 \times log_{10}\left(\frac{GMD^{neutral\,2}_{(m)}}{GMR^{neutral}_{(m)}\sqrt[3]{GMR^{phase}_{(m)}\left(GMD^{phase}_{(m)}\right)^2}}\right)\right\}, \quad (6)$$

where $R^{neutral}_{(m)}$ is the resistance of the neutral conductor (Ω/1000 ft). Equations (7) and (8) are approximations for the self ($Z^{self}_{(m)}$) and mutual ($Z^{mutual}_{(m)}$) impedances of the lines [22]:

$$Z^{self}_{(m)} = \frac{Z^0_{(m)} + 2Z^+_{(m)}}{3}, \quad (7)$$

$$Z^{mutual}_{(m)} = \frac{Z^0_{(m)} - Z^+_{(m)}}{3}. \quad (8)$$

Then, the simplification process is further carried out by assuming that the self-impedance terms are equal and that the mutual impedances are identical. This reasoning allows us to approximate the impedance matrix ($\mathbf{Z}_{(m)}$) using Equation (9) [22]:

$$\mathbf{Z}_{(m)} = \begin{bmatrix} Z^{self}_{(m)} & Z^{mutual}_{(m)} & Z^{mutual}_{(m)} \\ Z^{mutual}_{(m)} & Z^{self}_{(m)} & Z^{mutual}_{(m)} \\ Z^{mutual}_{(m)} & Z^{mutual}_{(m)} & Z^{self}_{(m)} \end{bmatrix}. \quad (9)$$

The analysis of a typical DS is an iterative process. For a specific iteration ($p = 1, \ldots, P$) of the power flow process, the vector of voltages ($\boldsymbol{V}_{(p)}$) and currents ($\boldsymbol{I}_{(p)}$)

at each bus, branch, and phase can be defined according to Equations (10) and estimated using Equations (11) and (12) [23]:

$$\boldsymbol{V}_{(p)} = \begin{bmatrix} V_{(1,p)} \\ \vdots \\ V_{(n,p)} \\ \vdots \\ V_{(3N,p)} \end{bmatrix}, \boldsymbol{I}_{(p)} = \begin{bmatrix} I_{(1,p)} \\ \vdots \\ I_{(n,p)} \\ \vdots \\ I_{(3N,p)} \end{bmatrix} \tag{10}$$

$$\boldsymbol{\Delta V}_{(p+1)} = \{\boldsymbol{BCBV} \times \boldsymbol{BIBC}\} \times \boldsymbol{I}_{(p)}, \tag{11}$$

$$\boldsymbol{V}_{(p+1)} = \boldsymbol{V_{sub}} + \boldsymbol{\Delta V}_{(p+1)}, \tag{12}$$

where $\boldsymbol{\Delta V}_{(p+1)}$ is the vector of variations of bus voltages, $\boldsymbol{BCBV}$ is the branch-current to bus-voltage matrix, $\boldsymbol{BIBC}$ is the bus-injection to branch-current matrix, and $\boldsymbol{V_{sub}}$ is a vector of values equal to the substation voltage. Equations (11) and (12) are sequentially applied until the error in the voltage estimation becomes negligible. The elements of the vector of current injection ($\boldsymbol{I}_{(p)}$) are obtained from the load apparent power and the corresponding bus and phase voltage properly conjugated. To calculate voltages and currents under unbalanced operating conditions, the $\boldsymbol{BIBC}$ matrix is expanded by replacing the scalar +1 elements with a 3 × 3 identity matrix. Similarly, in the $\boldsymbol{BCBV}$ matrix, the impedance value between two consecutive buses, originally associated with a single-phase system, is replaced by the corresponding impedance matrix $\boldsymbol{Z}_{(m)}$ with a 3 × 3 structure [23].

With regard to power generation from distributed generation units, it is commonly modeled as a negative active power injection operating at unity power factor. In contrast, the effect of an RPCD at a specific bus and phase is represented as a negative reactive power demand.

3. Optimal Sizing and Placement of Reactive Power Compensation

The optimal allocation of RPCDs is a challenging problem. On the one hand, it requires determining the appropriate amount of reactive power to be installed. On the other hand, it involves identifying the buses at which this reactive power should be deployed. Consequently, two distinct optimization tasks must be addressed. This research proposes the implementation of the EES to solve the optimal sizing and placement of RPCDs. In the following subsections, a brief overview of EES is presented, along with its application to the optimal dispatch and placement of reactive power.

3.1. Optimal Dimensioning and Placement of Reactive Power Compensation Devices

The optimal sizing and placement of RPCDs constitute two distinct yet interdependent problems. Consequently, solving the placement problem requires addressing the corresponding reactive power dispatch problem. To handle this interdependence, both problems are solved in a coordinated manner using the EES. On the one hand, the placement problem is formulated using binary encoding. On the other hand, the sizing problem is formulated using real-valued encoding. Accordingly, a population of binary agents or individuals ($\boldsymbol{X_{pop}^{binary}}$) is defined to address the placement problem, while a population of real-valued agents ($\boldsymbol{X_{pop}^{real}}$) is used to solve the reactive power dispatch problem.

The structure of each of these agents is illustrated in Figure 1. The population used to solve the placement problem ($\boldsymbol{X_{pop}^{binary}}$) consists of S rows, representing the total number of individuals, and N columns, corresponding to the number of buses in the system. With respect to the binary encoding, a value of zero indicates the absence of reactive power compensation, whereas a value of one indicates the installation of reactive power

compensation at the corresponding bus. As shown in Figure 1, an RPCD is connected at bus n, while bus N is not provided with compensation.

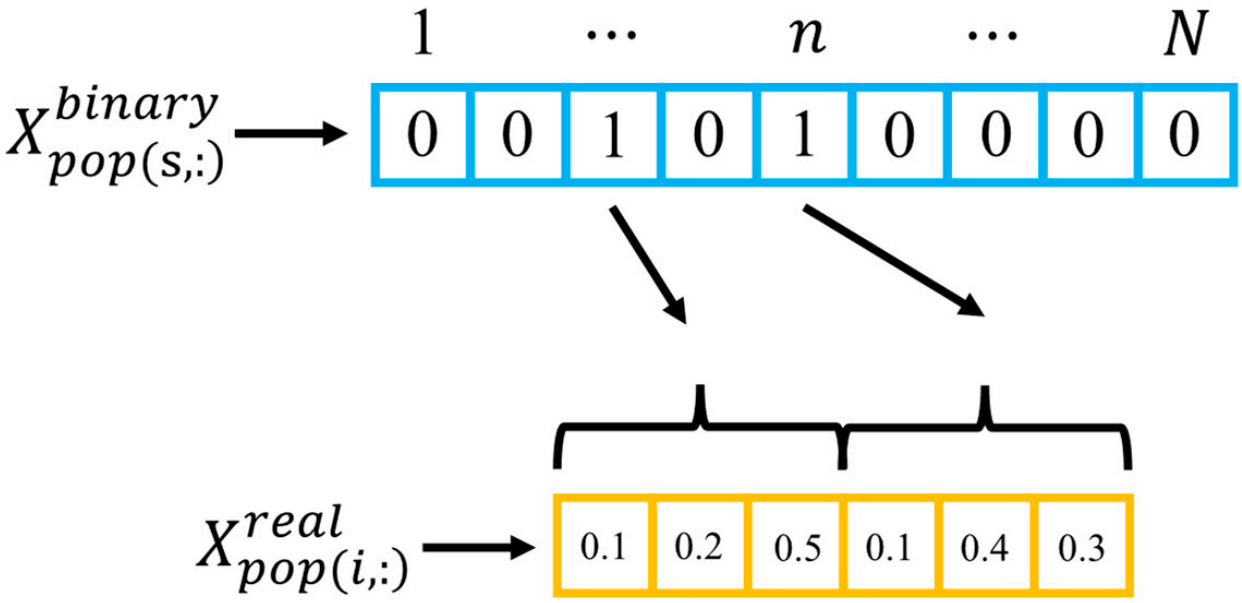

Figure 1. Optimization agents for the dispatch and placement of RPCDs.

Moreover, the population employed to solve the dispatch problem ($\boldsymbol{X}^{real}_{pop}$) consists of I rows, representing the number of individuals, and a number of columns that depends on the number of buses equipped with reactive power compensation. According to Figure 1, an RPCD is connected at bus n, and the reactive power injected in phases a, b, and c is 0.1, 0.4, and 0.3 per unit, respectively.

The following subsection briefly presents the mathematical formulation of the optimal reactive power dispatch problem (Section 3.1.1) and its solution using the EES (Section 3.1.2).

3.1.1. Problem Formulation for Optimal Reactive Power Dispatch

The optimal dispatch of RPCDs consists of determining the reactive power injection settings of each device in a cost-effective manner. To this end, the formulation presented in Equations (13)–(18) is adopted.

The objective function is defined in Equations (13) and (14) and aims to minimize the amount of reactive power injected into the system. It is formulated under the assumption that the associated cost is proportional to the injected reactive power.

$$min\left\{\sum_{r=1}^{R} X^{real}_{pop(i,r)}\right\}, \tag{13}$$

$$R = 3\sum_{n=1}^{N} X^{binary}_{pop(s,n)}. \tag{14}$$

The problem constraints are defined by Equations (15)–(18). Equation (15) imposes limits on the operating voltage at each bus and phase, while Equation (16) represents the ampacity constraints of each distribution line. Equations (17) and (18) are associated with the power-flow solution obtained through the iterative method described in reference [23].

$$V_{min} \leq \left|V_{(r,p)}\right| \leq V_{max} \; \forall \; r = 1, \ldots, R; \tag{15}$$

$$\left|I_{(r,p)}\right| \leq I_{(r)}^{max} \; \forall \; r = 1, \ldots, R; \tag{16}$$

$$\boldsymbol{V}_{(p+1)} = \boldsymbol{V_{sub}} + \{\boldsymbol{BCBV} \times \boldsymbol{BIBC}\} \times \boldsymbol{I}_{(p)}, \tag{17}$$

$$max\left\{\left|\boldsymbol{V}_{(p+1)} - \boldsymbol{V}_{(p)}\right|\right\} < \theta. \tag{18}$$

$$X_{min}^{real} \leq X_{pop(i,r)}^{real} \leq X_{max}^{real} \; \forall \; i = 1, \ldots, I; r = 1, \ldots, R. \tag{19}$$

With respect to the variables involved in Equations (13)–(14), $X_{pop(i,r)}^{real}$ denotes the r-th element ($r = 1, \ldots, R$) of agent or individual i ($i = 1, \ldots, I$) in the population $\boldsymbol{X_{pop}^{real}}$. Similarly, $X_{pop(s,n)}^{binary}$ represents the n-th element ($n = 1, \ldots, N$) of agent s ($s = 1, \ldots, S$) in the population $\boldsymbol{X_{pop}^{binary}}$. The variable θ is the tolerance associated with the power flow calculation. Equation (19) ensures the feasibility of the solution by constraining the reactive power to lie between zero and one. Accordingly, X_{min}^{real} is set to zero, and X_{max}^{real} is set to one.

3.1.2. Optimal Reactive Power Dispatch Using the Experience Exchange Strategy

The EES is computationally implemented through the following steps:

Step 1. The population $\boldsymbol{X_{pop}^{real}}$ is initialized using uniformly distributed random numbers. Specifically, small values in the range from 0 to 0.001 are employed.

Step 2. The initial population is evaluated by performing a power-flow study that considers the reactive power injection of each agent ($i = 1, \ldots, I$) in the population. The objective function $F_{obj(i)}^{real}$ is defined in Equations (20)–(22):

$$F_{obj(i)}^{real} = \sum_{r=1}^{R} X_{pop(i,r)}^{real} + X_{penalty(r)}^{voltage} + X_{penalty(r)}^{current} \tag{20}$$

$$X_{penalty(r)}^{voltage} = \begin{cases} 0; if\left(\left|V_{(r,p)} - V_{sub}\right| < \lambda\right) \\ X_{penalty}^{max} \times exp\left(\left|\lambda - \left|V_{(r,p)} - V_{sub}\right|\right|\right); otherwise \end{cases}, \tag{21}$$

$$X_{penalty(r)}^{current} = \begin{cases} 0; if\left(I_{(r,p)} < I_{(r)}^{max}\right) \\ X_{penalty}^{max} \times exp\left(I_{(r,p)} - I_{(r)}^{max}\right); otherwise \end{cases}, \tag{22}$$

where $X_{pop(i,r)}^{real}$ is associated with Equation (13), while $X_{penalty(r)}^{voltage}$ and $X_{penalty(r)}^{current}$ are penalty factors related to Equations (15) and (16), respectively. The parameter $X_{penalty}^{max}$ is set to a large value; in this study, a value of 99,999 is adopted. Moreover, the parameter λ is associated with a voltage variation of $\pm 5\%$, that is, $\lambda = 0.05$. V_{sub} denotes the substation voltage, and $I_{(r)}^{max}$ represents the ampacity of conductor r.

Step 3. Perform the first iteration by setting k←1. Then, proceed to Step 4.

Step 4. If $k \leq K$, where K is the maximum number of iterations, go to Step 5, else end.

Step 5. Apply the experience exchange formula of Equation (23) [24]. Then, go to Step 6.

$$X_{pop(:,r)}^{ee} = \begin{cases} X_{pop(\boldsymbol{RND_2},r)}^{real}; if(RND_1 < 0.85) \\ X_{pop(:,r)}^{real}; otherwise \end{cases} \quad \forall \; r = 1, \ldots, R \tag{23}$$

where $\boldsymbol{X_{pop}^{ee}}$ is a matrix containing the experience exchange of the most recent strategies. It consists of I rows and R columns. RND_1 is a uniformly distributed random number in the interval [0,1], and $\boldsymbol{RND_2}$ is a vector of integer-valued random numbers of length I, with elements drawn from the interval [1,I].

Step 6. If $k \leq \lfloor 0.5 \times K \rfloor$, proceed to Step 7; otherwise, proceed to Step 12.

Step 7. Apply the experience scarcity stage (ESC) according to Equations (24) and (25) [24]. Then, go to Step 8.

$$\begin{cases} u = X^{ee}_{pop(RND_3,:)} \\ v = X^{ee}_{pop(RND_4,:)} \\ c = \left(\frac{1}{1-K}\right)k - \frac{K}{1-K} \end{cases}, \tag{24}$$

$$X^{esc}_{pop(i,:)} = X^{real}_{pop(i,:)} + (u - v). \times c \; \forall \; i = 1, \ldots, I, \tag{25}$$

where RND_3 and RND_4 are integer-valued random numbers in the interval [1,I], and $\boldsymbol{X^{esc}_{pop}}$ denotes the population obtained from the ESC.

Step 8. Enforce the elements of $\boldsymbol{X^{esc}_{pop}}$ to satisfy the constraints of Equation (19). Then, proceed to Step 9.

Step 9. Compute the objective function values of the population $\boldsymbol{X^{esc}_{pop}}$ in accordance with Equations (20)–(22) by performing a power-flow analysis. Then, proceed to Step 10.

Step 10. Select the best individual i ($i = 1, \ldots, I$) by comparing the population $\boldsymbol{X^{real}_{pop}}$ at the current iteration k with the population $\boldsymbol{X^{esc}_{pop}}$ obtained from the ESC. Go to Step 11.

Step 11. Set $k \leftarrow k + 1$ and proceed to Step 4.

Step 12. If ($k > \lfloor 0.5 \times K \rfloor$ and $k \leq \lfloor 0.8 \times K \rfloor$) proceed to Step 13; otherwise, proceed to Step 18.

Step 13. Apply the experience crossover stage (ECR) according to Equations (26) and (27) [24]. Then, go to Step 14.

$$\begin{cases} u = X^{ee}_{pop(RND_5,:)} \\ v = X^{ee}_{pop(RND_6,:)} \\ w = X^{ee}_{pop(RND_7,:)} \\ c = \left(\frac{1}{1-K}\right)k - \frac{K}{1-K} \end{cases} \tag{26}$$

$$X^{ecr}_{pop(i,:)} = X_{pop(i,:)} + (u - v). \times \boldsymbol{RND_8} + (u - w). \times (1 - \boldsymbol{RND_9}). \times c \tag{27}$$

where RND_5, RND_6, and RND_7 are integer random numbers in the interval [1,I], while $\boldsymbol{RND_8}$ and $\boldsymbol{RND_9}$ are vectors of uniform random numbers of length R.

Step 14. Enforce the elements of $\boldsymbol{X^{ecr}_{pop}}$ to satisfy the constraints of Equation (19). Then, proceed to Step 15.

Step 15. Compute the objective function values of the population $\boldsymbol{X^{ecr}_{pop}}$ in accordance with Equations (20)–(22) by performing a power-flow analysis. Then, proceed to Step 16.

Step 16. Select the best individual i ($i = 1, \ldots, I$) by comparing the population $\boldsymbol{X^{real}_{pop}}$ at the current iteration k with the population $\boldsymbol{X^{ecr}_{pop}}$ obtained from the ECR. Go to Step 17.

Step 17. Set $k \leftarrow k + 1$ and proceed to Step 4.

Step 18. If ($k > \lfloor 0.8 \times K \rfloor$) proceed to Step 19.

Step 19. Apply the experience sharing stage (ESH) according to Equations (28) and (29) [24]. Then, go to Step 20.

$$\begin{cases} u = X^{ee}_{pop(RND_8,:)} \\ v = X^{ee}_{pop(RND_9,:)} \\ w = X^{ee}_{pop(RND_{10},:)} \\ c = \left(\frac{1}{1-K}\right)k - \frac{K}{1-K} \end{cases} \tag{28}$$

$$X^{esh}_{pop(i,:)} = \left(X_{pop(i,:)} - w\right)./2 + (u - v). \times \boldsymbol{RND_{11}}. \times c \tag{29}$$

where RND_8, RND_9, and RND_{10} are integer random numbers in the interval [1,I], while $\boldsymbol{RND_{11}}$ is a vector of uniform random numbers with R elements.

Step 20. Enforce the elements of $\boldsymbol{X}_{pop}^{esh}$ to satisfy the constraints of Equation (19). Then, proceed to Step 21.

Step 21. Compute the objective function values of the population $\boldsymbol{X}_{pop}^{esh}$ in accordance with Equations (20)–(22) by performing a power-flow analysis. Then, proceed to Step 22.

Step 22. Set $k \leftarrow k+1$ and proceed to Step 4.

The operators $.\times$ and $./$ denote element-wise multiplication and division, respectively. These operations involve multiplying or dividing each element of a vector by a scalar, or performing multiplication or division between corresponding elements of two vectors of equal length.

3.1.3. Optimal Placement of Reactive Power Compensation Devices Using the Experience Exchange Strategy

In this subsection, attention is focused on the portion of the algorithm devoted to determining the appropriate connection buses for the RPCDs. As illustrated in Figure 1, this corresponds to a binary-coded version of the EES, in which the population is represented by the matrix $\boldsymbol{X}_{pop}^{binary}$, consisting of S individuals and N columns. Since the original EES is formulated using real-valued encoding, it is necessary to convert the real-coded individuals into binary ones. To this end, Equation (30) is applied:

$$X_{pop(s,n)}^{binary} = \begin{cases} 0; if(\alpha < 0.5) \\ 1; otherwise \end{cases} \quad \forall\, n = 1, \ldots, N; \quad s = 1, \ldots S; \tag{30}$$

where α is the real-valued parameter obtained during the implementation of the EES, which must be converted into a binary value. Once the population corresponding to the placement problem $\boldsymbol{X}_{pop}^{binary}$ has been obtained, this result is used to compute the objective function value, which is determined by solving the optimal dispatch problem described in Sections 3.1.1 and 3.1.2. In other words, for each individual in the optimal placement problem, the corresponding optimal dispatch problem must be solved. Consequently, the two optimization problems are interconnected. It is important to note that the remaining stages of the EES are applied using the associated real-valued parameters (α) corresponding to the elements $X_{pop(s,n)}^{binary}$.

3.1.4. Optimal Placement and Sizing of Reactive Power Compensation Devices Using the Experience Exchange Strategy

EES has been used flexibly to solve both integer- and real-coded problems. Specifically, integer coding has been employed to search for the optimal locations of RPCDs, while real coding has been used to determine their optimal reactive power dispatch. Since the condition of maximum load is considered, it provides valuable information directly related to the reactive power injection rating.

The general process is depicted in Figures 2 and 3 for optimal placement and sizing, respectively. According to Figure 2, the experience scarcity (ESC), crossover (ECR), and sharing (ESH) operators are applied depending on the evolution of the optimization process, which is represented by the corresponding iteration. Another relevant step is the transformation of real numbers into binary values, which are required to assess the fitness of each agent. This process is carried out by re-implementing EES with real coding. Thus, the placement and sizing optimization problems are nested.

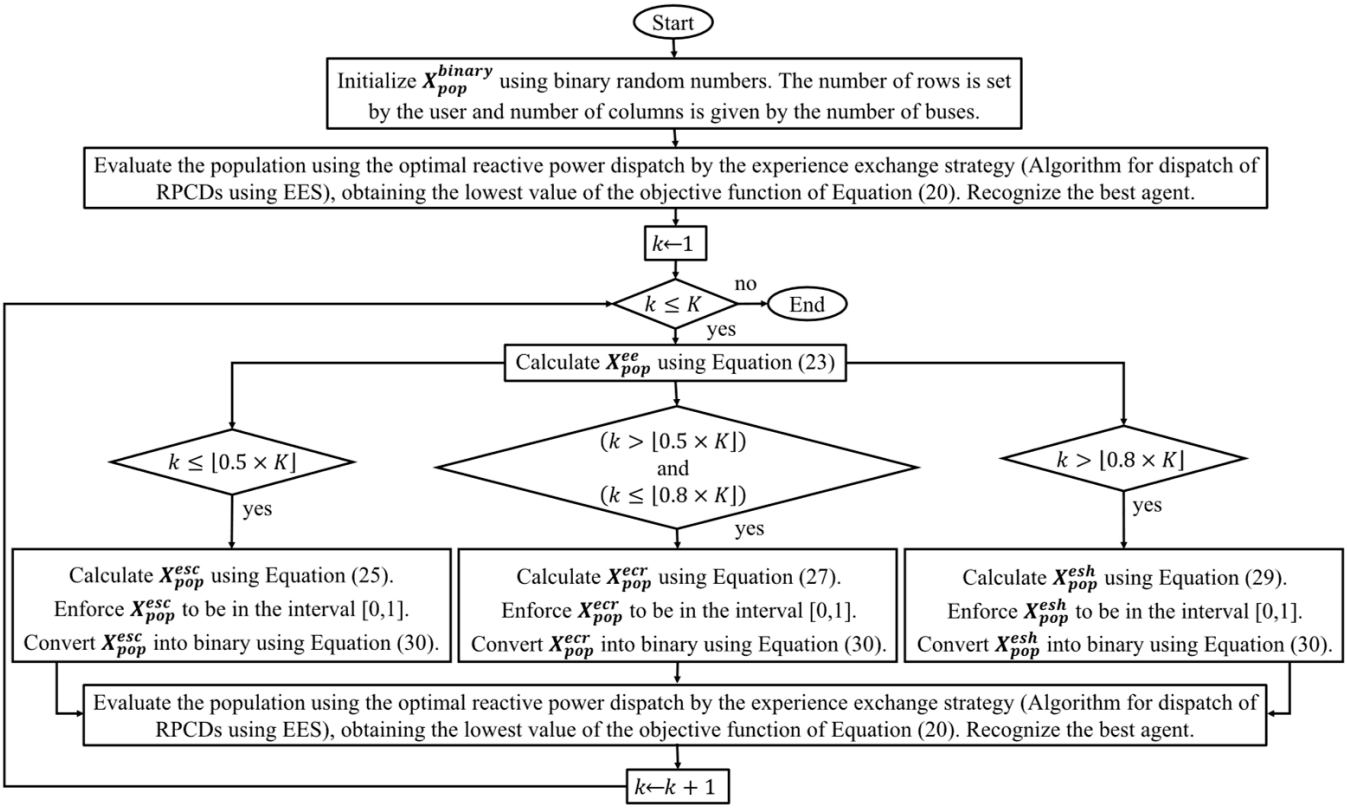

Figure 2. Algorithm for placement of RPCDs using EES.

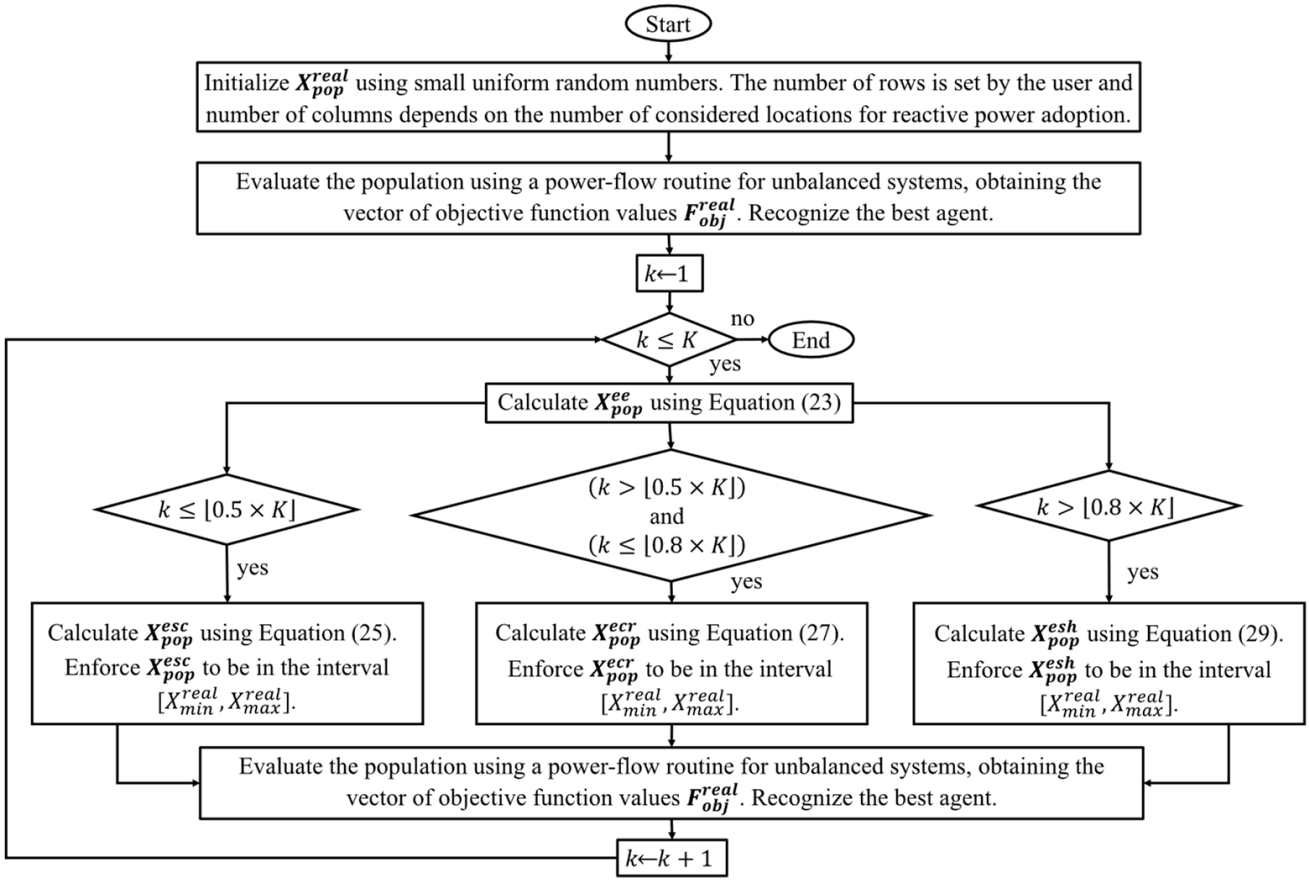

Figure 3. Algorithm for dispatch of RPCDs using EES.

In the next section, the proposed methodology is illustrated through two case studies.

4. Case Studies

The methodology proposed in this work for the optimal placement and sizing of RPCDs using the EES is evaluated through two case studies. It was implemented in the MATLAB® version R2024b programming language on a personal computer provided with an Intel® Core™ i7-10700 CPU @ 2.90 GHz with 32 GB of RAM (Intel Corporation, Santa Clara, CA, USA). In both cases, the geometric mean distance and geometric mean radius of the phase conductor are $GMD_{(m)}^{phase}$ = 4.8 ft and $GMD_{(m)}^{neutral}$ = 6.3 ft, respectively. The earth resistivity is set to ρ_{earth} = 100 Ωm. The maximum number of iterations for solving the power flow is set to 15 (P = 15), with an associated tolerance of 0.001 (θ = 0.001). The minimum and maximum allowable operating voltages, expressed in per unit, are (V_{min} = 0.95 p.u.) and (V_{max} = 1.05 p.u.), respectively. The substation voltage is set to 1 p.u.; therefore, the vector $\boldsymbol{V_{sub}}$ is defined as a vector of ones. In the first case, a system with 15 buses is studied, whereas in the second case, the system of interest has 70 buses. The complete analysis of each network is presented in Sections 4.1 and 4.2.

4.1. Characteristics of the 15-Bus Distribution System

The system consists of 15 buses ($n = 1, \ldots, N$ = 15) and the same number of overhead distribution lines ($m = 1, \ldots, M$ = 15). The network configuration is shown in Figure 4 and corresponds to a four-wire multigrounded system using aluminum conductor steel reinforced (ACSR) cables rated at 75 °C. The nominal voltage is 13.8 kV, and the substation capacity is 8000 kVA.

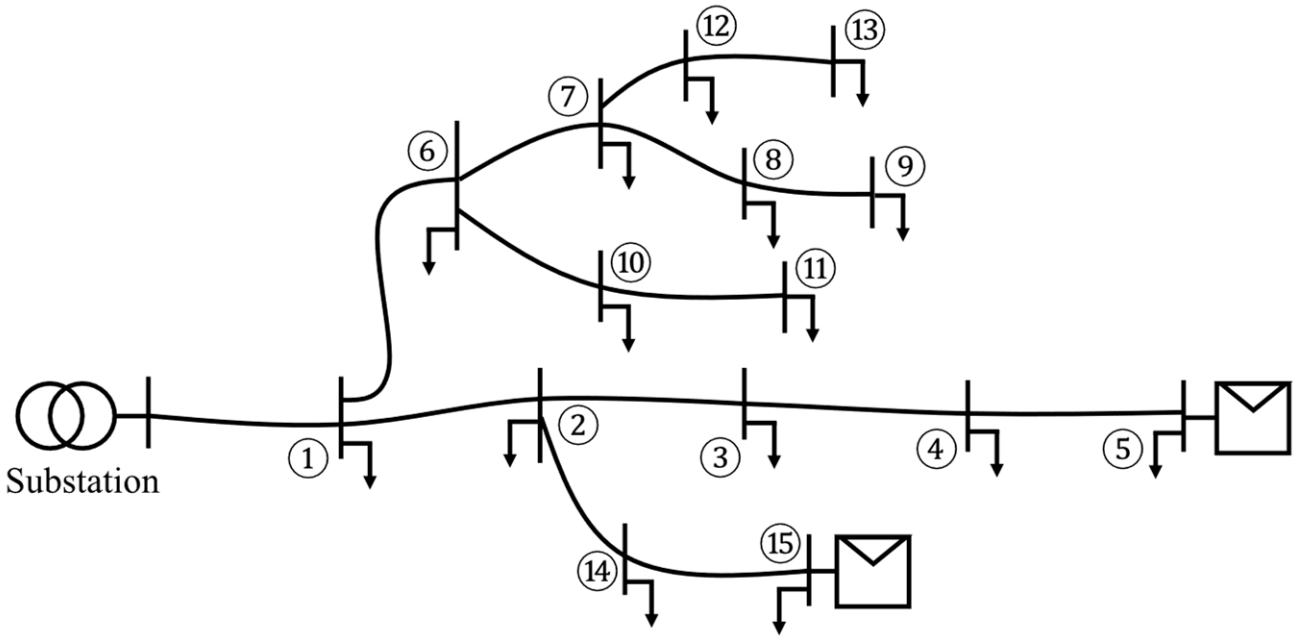

Figure 4. Distribution network with 15 buses.

The general characteristics of the distribution lines and the maximum active load per phase are presented in Table 2, including the sizes of the phase and neutral conductors, their ampacity ratings, and the feeder lengths. The corresponding reactive power values of the maximum load are calculated assuming a power factor of 0.85.

Table 2. Characteristics of the distribution lines and load demand in the 15-bus system.

Sending Node	Receiving Node	Phase and Neutral Conductors (kcmil)	Ampacity (A)	Length (ft)	Load Per Phase [a,b,c] (kW)
Substation	1	83.69	134	8809	[159,154,139]
1	2	83.69	134	8305	[135,145,139]
2	3	83.69	134	9685	[159,160,136]
3	4	83.69	134	8325	[154,156,149]
4	5	83.69	134	9001	[138,148,143]
1	6	41.74	83	9403	[203,171,178]
6	7	41.74	83	8727	[180,195,205]
7	8	41.74	83	8298	[190,195,181]
8	9	41.74	83	9350	[176,195,205]
6	10	41.74	83	8614	[184,171,173]
10	11	41.74	83	8826	[179,169,191]
7	12	41.74	83	9610	[176,190,183]
12	13	41.74	83	8210	[169,195,179]
2	14	41.74	83	9334	[133,111,115]
14	15	41.74	83	9663	[131,134,114]

The following subsections analyze the actual operating conditions of the system (Section 4.1.1), present the results of the optimal dispatch of reactive power compensation (Section 4.1.2), and subsequently illustrate the results obtained from the optimal placement procedure (Section 4.1.3).

4.1.1. Assessment of the Preliminary Conditions of the 15-Bus System

To assess the benefits associated with the adoption of RPCDs, this subsection analyzes the system under its actual operating conditions without any reactive power compensation in service. Furthermore, the system is assumed to operate under the heaviest loading conditions, corresponding to the maximum load values reported in Table 2, with no contribution from the distributed generation connected at buses 5 and 15. Accordingly, Table 3 presents the phase voltages and currents. On the one hand, the voltage magnitudes range from 0.847 p.u. to 0.9539 p.u., with the minimum voltage magnitude falling below the desired operating interval of 0.95 p.u. On the other hand, the maximum current is 0.0355 p.u., which is lower than the corresponding conductor ampacity and therefore does not constitute an operational constraint.

Table 3. Voltage and current magnitudes per bus and phase under actual conditions for the 15-bus system.

Bus or Branch	Voltage Phase a (p.u.)	Voltage Phase b (p.u.)	Voltage Phase c (p.u.)	Current Phase a (p.u.)	Current Phase b (p.u.)	Current Phase c (p.u.)	Ampacity (p.u.)
1	0.9536	0.9523	0.9539	0.0245	0.0238	0.0214	0.4004
2	0.9391	0.9373	0.9405	0.0211	0.0227	0.0217	0.4004
3	0.9301	0.9276	0.9321	0.0251	0.0254	0.0215	0.4004
4	0.9251	0.9223	0.9270	0.0245	0.0249	0.0236	0.4004
5	0.9226	0.9195	0.9243	0.0220	0.0237	0.0227	0.4004
6	0.9026	0.8999	0.9006	0.0331	0.0279	0.0291	0.2480
7	0.8737	0.8676	0.8683	0.0303	0.0330	0.0347	0.2480
8	0.8623	0.8552	0.8559	0.0324	0.0335	0.0311	0.2480
9	0.8562	0.8483	0.8483	0.0302	0.0338	0.0355	0.2480
10	0.8909	0.8893	0.8891	0.0304	0.0283	0.0286	0.2480

Table 3. *Cont.*

Bus or Branch	Voltage Phase a (p.u.)	Voltage Phase b (p.u.)	Voltage Phase c (p.u.)	Current Phase a (p.u.)	Current Phase b (p.u.)	Current Phase c (p.u.)	Ampacity (p.u.)
11	0.8850	0.8840	0.8828	0.0297	0.0281	0.0318	0.2480
12	0.8614	0.8533	0.8548	0.0300	0.0327	0.0315	0.2480
13	0.8563	0.8470	0.8491	0.0290	0.0338	0.0310	0.2480
14	0.9303	0.9291	0.9333	0.0210	0.0176	0.0181	0.2480
15	0.9259	0.9243	0.9296	0.0208	0.0213	0.0180	0.2480

4.1.2. Analysis of the Optimal Reactive Power Dispatch in the 15-Bus System

Since two distinct optimization problems are addressed, this section presents the results corresponding to the optimal dispatch of reactive power for a given set of installation buses. In other words, the optimal reactive power dispatch—formulated as a real-coded optimization problem—is determined by considering the installation buses specified in Equation (31):

$$X_{pop(1,n)}^{binary} = \begin{cases} 1; if(n = 1 \bigvee n = 2 \bigvee n = 3 \bigvee n = 6 \bigvee n = 8) \\ 0; otherwise \end{cases} \quad \forall\, n = 1, \ldots, 15 \tag{31}$$

According to this expression, only buses 1, 2, 3, 6, and 8 are considered for reactive power compensation. The EES is implemented using a population size of 100 individuals (I = 100) and a maximum number of iterations of 150 (K = 150). For comparative purposes, a real-coded version of the GA [25,26] is also employed, using a proportional parameter of 0.3, crossover and mutation probabilities of 0.95 and 0.1, respectively, while maintaining the same population size and maximum number of iterations as those adopted for the EES implementation.

Figure 5 illustrates the evolution of the EES and the GA in determining the optimal dispatch of reactive power installed according to Equation (31). As observed at the final iteration (K = 150), the GA attains an objective function value of 417,900, whereas the EES achieves a considerably lower value of 108,152. The objective function values are high in both cases because the corresponding solutions are infeasible. In other words, the objective function is strongly influenced by the penalty term $X_{penalty}^{max} \approx 99{,}999$. The only way to obtain a feasible solution is by modifying the installation buses, whose configuration is represented by the vector $X_{pop(1,n)}^{binary}$ for all $n = 1, \ldots, N = 15$. This issue is addressed in the following subsection.

The solutions corresponding to Figure 5 are presented in Tables 4 and 5 for the EES and GA, respectively. In general, the reactive power injection suggested by the GA is higher than that proposed by the EES.

Table 4. Results of the optimal RPCD dispatch using EES for the 15-bus system.

Bus	Reactive Power Phase a (kVAr)	Reactive Power Phase b (kVAr)	Reactive Power Phase c (kVAr)
1	1989.0	2827.4	545.3
2	2180.3	975.1	1622.4
3	1166.0	2088.1	1929.8
6	1911.6	2063.2	2674.5
8	1700.6	1549.1	1766.4

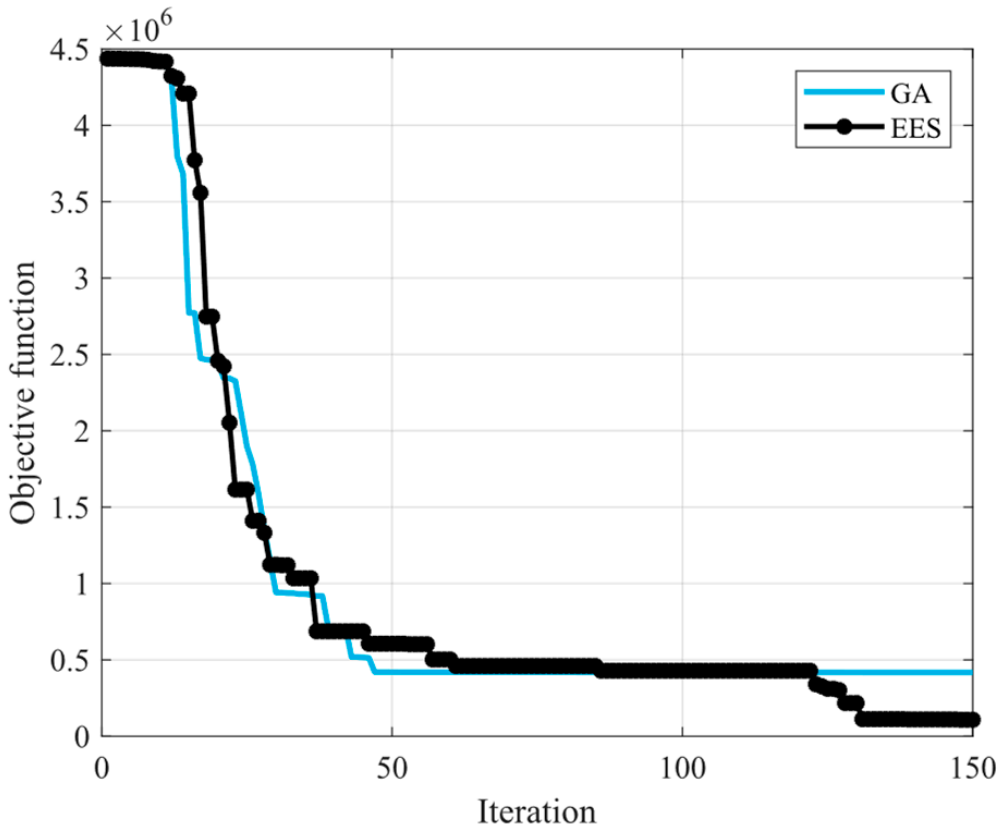

Figure 5. Evolution of EES and GA during the optimal reactive power dispatch for the 15-bus system.

Table 5. Results of the optimal RPCD dispatch using the GA for the 15-bus system.

Bus	Reactive Power Phase a (kVAr)	Reactive Power Phase b (kVAr)	Reactive Power Phase c (kVAr)
1	295.9	2123.6	2772.5
2	2946.3	1789.6	2500.2
3	1547.2	1059.5	1516.6
6	2794.7	2036.6	1543.1
8	1967.2	1648.5	2616.9

4.1.3. Determination of the Optimal Placement of Reactive Power Compensation Devices in the 15-Bus System

Once the results of the optimal reactive power dispatch have been discussed, the results of the optimal placement of RPCDs are presented. In this problem, the population size is set to 50 individuals, and the maximum number of iterations is set to 100. These parameter settings are applied to both algorithms, namely the EES and the GA.

An important limitation of heuristic optimization algorithms is the absence of analytical guarantees regarding the quality of the obtained solutions. In other words, these algorithms may provide high-quality solutions without assurance of global optimality, which is often associated with stagnation around local optima. To address this issue, the optimization procedure is repeated multiple times in order to explore the search space more thoroughly and increase the likelihood of identifying the global optimum. In this study, the computational optimization process is repeated 200 times.

Figure 6 presents the evolution of the optimization process performed by the EES, in which the experiment yielding the best result is highlighted in bold. The objective function value obtained in this experiment is 2.034, which corresponds to a feasible design. The specific characteristics of this solution are presented in Table 6, while the associated voltage

and current values are reported in Table 7, respectively. According to Table 7, the voltage magnitudes range from 0.9501 p.u. to 0.9824 p.u., which lie within the desired operating interval of 0.95 p.u. to 1.05 p.u. Moreover, the maximum current is 0.2031 p.u., which is lower than the corresponding ampacity limit.

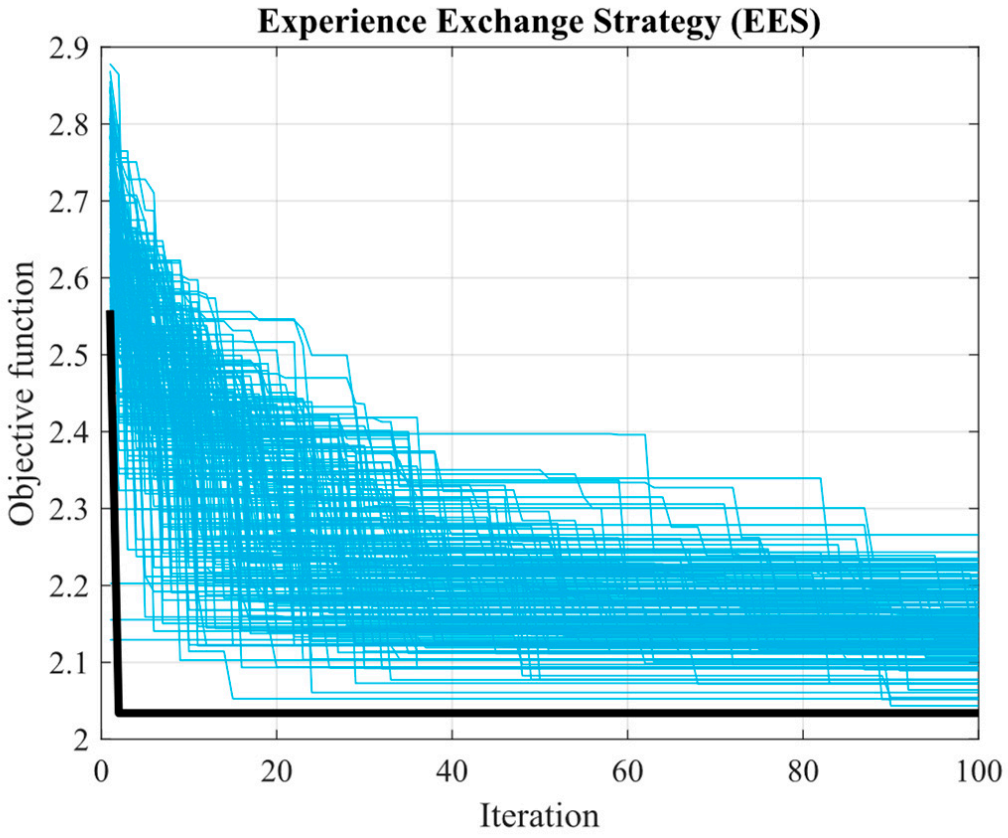

Figure 6. Evolution of the EES over 200 experiments for the 15-bus system.

Table 6. Results of the optimal RPCD placement using the EES for the 15-bus system.

Bus	Reactive Power Phase a (kVAr)	Reactive Power Phase b (kVAr)	Reactive Power Phase c (kVAr)
6	1165.7	1466.3	1392.5
7	1606.4	1187.9	1673.5
9	690.9	792.7	820.8
11	1175.4	1230.0	906.6
13	716.2	833.7	613.7

Figure 7 illustrates the evolution of the GA, with the experiment yielding the best result highlighted in bold. For this experiment, the objective function value is 2.197. Table 8 presents the characteristics of the proposed RPCD configuration, while Table 9 reports the voltage and current values obtained from the implementation of this solution. According to Table 9, the minimum and maximum voltage magnitudes are 0.95 p.u. and 0.988 p.u., respectively, which lie within the desired operating interval. Moreover, the maximum current is 0.1095 p.u., which is lower than the corresponding ampacity limit.

Table 7. Voltage and current magnitudes per bus and phase using EES for the 15-bus system.

Bus or Branch	Voltage Phase a (p.u.)	Voltage Phase b (p.u.)	Voltage Phase c (p.u.)	Current Phase a (p.u.)	Current Phase b (p.u.)	Current Phase c (p.u.)	Ampacity (p.u.)
1	0.9818	0.9821	0.9824	0.0238	0.0231	0.0208	0.4004
2	0.9677	0.9675	0.9694	0.0205	0.0220	0.0211	0.4004
3	0.9590	0.9582	0.9612	0.0244	0.0245	0.0208	0.4004
4	0.9542	0.9531	0.9564	0.0237	0.0240	0.0229	0.4004
5	0.9517	0.9503	0.9537	0.0213	0.0229	0.0220	0.4004
6	0.9658	0.9673	0.9651	0.1370	0.1771	0.1675	0.2480
7	0.9609	0.9570	0.9597	0.1958	0.1416	0.2031	0.2480
8	0.9551	0.9522	0.9548	0.0292	0.0301	0.0279	0.2480
9	0.9548	0.9535	0.9554	0.0795	0.0917	0.0946	0.2480
10	0.9646	0.9667	0.9593	0.0280	0.0260	0.0265	0.2480
11	0.9697	0.9720	0.9590	0.1391	0.1464	0.1056	0.2480
12	0.9564	0.9522	0.9516	0.0270	0.0293	0.0283	0.2480
13	0.9576	0.9538	0.9501	0.0828	0.0968	0.0702	0.2480
14	0.9592	0.9596	0.9624	0.0204	0.0170	0.0176	0.2480
15	0.9550	0.9550	0.9588	0.0202	0.0206	0.0175	0.2480

Table 8. Results of the optimal RPCD placement using the GA for the 15-bus system.

Bus	Reactive Power Phase a (kVAr)	Reactive Power Phase b (kVAr)	Reactive Power Phase c (kVAr)
3	655.6	876.2	507.7
6	543.4	790.4	898.4
8	644.7	684.8	634.8
9	925.9	848.9	848.2
10	701.7	843.9	825.2
11	527.1	414.5	381.3
12	476.9	458.2	612.7
13	830.8	734.5	661.5
14	297.8	466.2	485.5

Table 9. Voltage and current magnitudes per bus and phase using GA for the 15-bus system.

Bus or Branch	Voltage Phase a (p.u.)	Voltage Phase b (p.u.)	Voltage Phase c (p.u.)	Current Phase a (p.u.)	Current Phase b (p.u.)	Current Phase c (p.u.)	Ampacity (p.u.)
1	0.9828	0.9888	0.9852	0.0238	0.0229	0.0207	0.4004
2	0.9749	0.9852	0.9778	0.0204	0.0216	0.0209	0.4004
3	0.9722	0.9844	0.9719	0.0745	0.1007	0.0572	0.4004
4	0.9674	0.9794	0.9671	0.0234	0.0234	0.0227	0.4004
5	0.9650	0.9767	0.9645	0.0210	0.0223	0.0218	0.4004
6	0.9586	0.9675	0.9639	0.0605	0.0911	0.1048	0.2480
7	0.9504	0.9545	0.9522	0.0278	0.0300	0.0317	0.2480
8	0.9512	0.9538	0.9510	0.0736	0.0782	0.0727	0.2480
9	0.9537	0.9542	0.9511	0.1095	0.0987	0.0985	0.2480
10	0.9569	0.9671	0.9619	0.0804	0.0979	0.0960	0.2480
11	0.9564	0.9649	0.9587	0.0592	0.0457	0.0424	0.2480
12	0.9500	0.9506	0.9508	0.0536	0.0513	0.0699	0.2480
13	0.9523	0.9500	0.9500	0.0979	0.0847	0.0762	0.2480
14	0.9679	0.9820	0.9751	0.0327	0.0525	0.0551	0.2480
15	0.9636	0.9775	0.9715	0.0200	0.0202	0.0173	0.2480

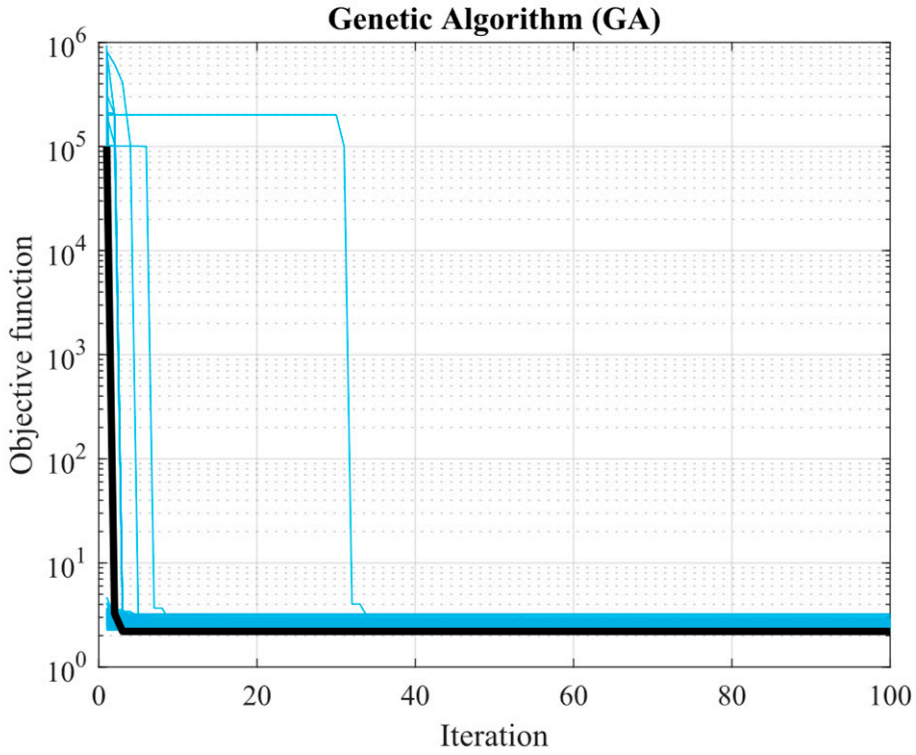

Figure 7. Evolution of the GA over 200 experiments for the 15-bus system.

Figure 8 presents the histogram of frequencies constructed from the 200 solutions obtained in Figures 6 and 7 for the EES and GA, respectively. Based on this information, it can be observed that the EES is capable of reaching better local minima than the GA. This histogram also enables the estimation of the probability of finding an improved solution by repeating the optimization process. Such a probability is estimated using the methodology proposed by Finch et al. [27] and is reported in Table 10.

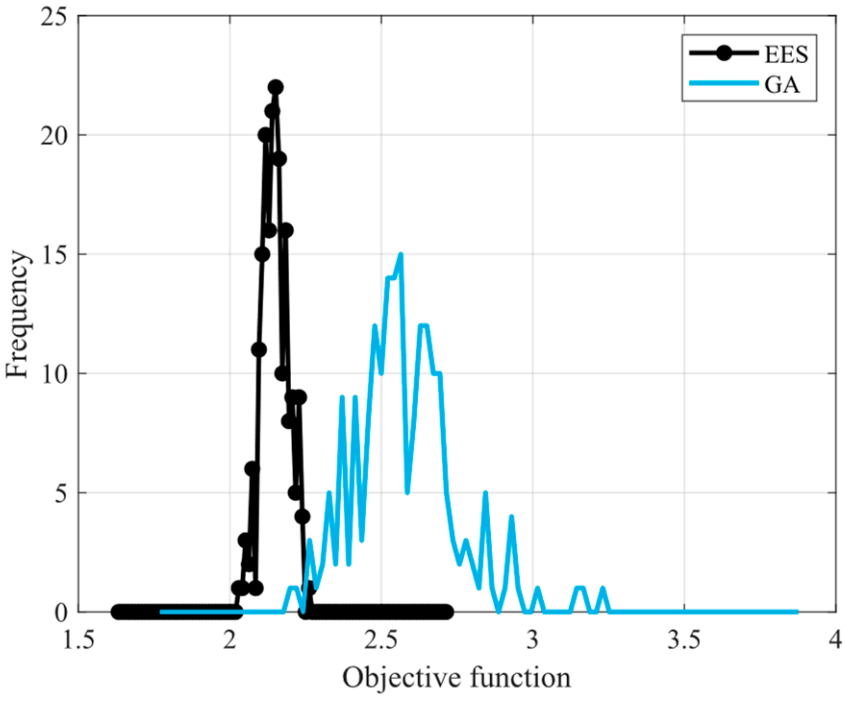

Figure 8. Histogram of the objective function for the 15-bus system.

Table 10. Expected probability of finding a new local optimum for the 15-bus system.

Optimization Method	Probability
EES	0.0206
GA	0.0569

According to Table 10, for the EES, the probability of identifying a new local optimum by repeating the optimization process is 2.06%. Therefore, the likelihood that all local minima have already been observed is high. In contrast, for the GA, this probability is slightly higher, at 5.69%, indicating that extending the optimization process may lead to the discovery of the solution obtained by the EES or potentially an even better one. In any case, both solutions exhibit high-quality characteristics.

Regarding the computational time, each computational experiment required approximately one hour.

Figure 9 summarizes the results previously reported in Tables 3 and 7 in graphical form for each bus shown in Figure 4. The improvement in the voltage profile resulting from the incorporation of RPCDs is clearly shown. However, it can be observed that the voltage per phase at a specific bus remains different among them.

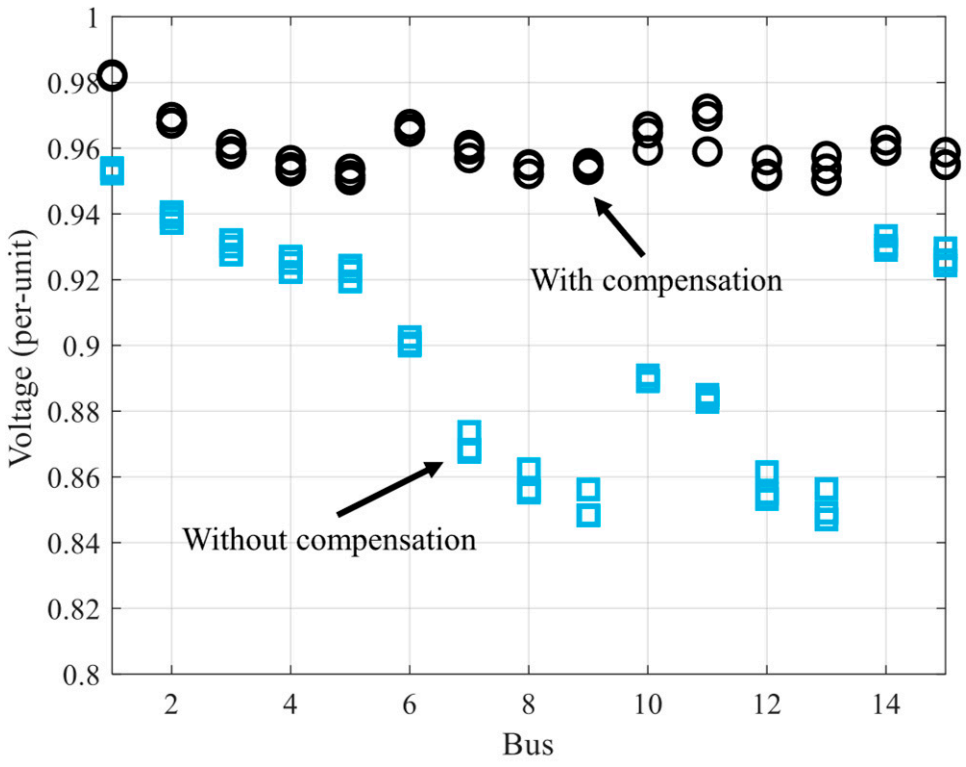

Figure 9. Voltage profile of the 15-bus system.

4.2. Characteristics of the 70-Bus Distribution System

The system consists of 70 buses (N = 70) and 70 branches (M = 70). The network configuration is shown in Figure 10 and corresponds to a four-wire multigrounded system using all-aluminum conductor (AAC) cables rated at 75 °C. The nominal voltage is 12.47 kV, and the substation capacity is 7500 kVA.

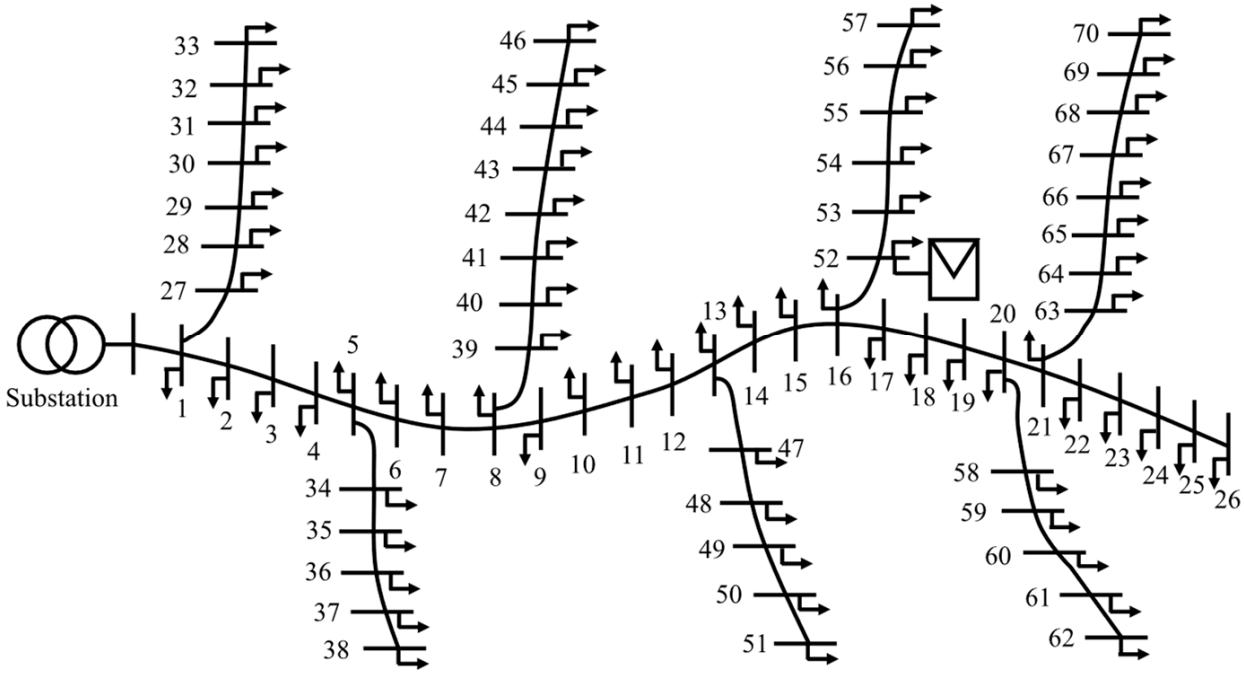

Figure 10. Distribution network with 70 buses.

The general characteristics of the distribution lines and the maximum active load per phase are summarized in Table 11. This table includes the sizes of the phase and neutral conductors, their corresponding ampacity ratings, and the feeder lengths. The reactive power associated with the maximum load is calculated assuming a power factor of 0.90.

Table 11. Characteristics of the distribution lines and load demand in the 70-bus system.

Sending Node	Receiving Node	Phase and Neutral Conductors (kcmil)	Ampacity (A)	Length (ft)	Load Per Phase [a,b,c] (kW)
Substation	1	211.6	254	3173	[12,13,8]
1	2	211.6	254	3321	[10,10,7]
2	3	211.6	254	3140	[9,9,13]
3	4	211.6	254	3070	[8,10,9]
4	5	211.6	254	2902	[8,13,8]
5	6	211.6	254	2922	[11,7,11]
6	7	211.6	254	2902	[12,8,9]
7	8	211.6	254	3126	[7,8,9]
8	9	211.6	254	2872	[11,10,13]
9	10	211.6	254	3223	[13,11,13]
10	11	211.6	254	3393	[11,9,8]
11	12	211.6	254	3472	[8,10,11]
12	13	211.6	254	3462	[11,12,11]
13	14	211.6	254	3170	[13,13,13]
14	15	211.6	254	3197	[7,10,13]
15	16	211.6	254	3236	[10,10,10]
16	17	211.6	254	2826	[11,12,10]
17	18	211.6	254	3299	[7,11,7]
18	19	211.6	254	3418	[11,13,13]
19	20	211.6	254	2826	[9,13,10]
20	21	211.6	254	3286	[12,13,9]
21	22	211.6	254	3328	[11,9,8]

Table 11. *Cont.*

Sending Node	Receiving Node	Phase and Neutral Conductors (kcmil)	Ampacity (A)	Length (ft)	Load Per Phase [a,b,c] (kW)
22	23	211.6	254	2985	[9,9,8]
23	24	211.6	254	3335	[12,8,9]
24	25	211.6	254	3071	[13,11,9]
25	26	211.6	254	2904	[8,8,7]
1	27	105.6	157	3341	[37,32,32]
27	28	105.6	157	3081	[35,32,32]
28	29	105.6	157	2831	[37,34,35]
29	30	105.6	157	3049	[37,37,33]
30	31	105.6	157	2882	[34,35,31]
31	32	105.6	157	3331	[35,32,32]
32	33	105.6	157	3140	[34,32,37]
5	34	105.6	157	3483	[47,48,50]
34	35	105.6	157	3177	[50,50,49]
35	36	105.6	157	3403	[48,50,50]
36	37	105.6	157	3396	[52,47,49]
37	38	105.6	157	3019	[51,50,52]
8	39	105.6	157	3263	[11,14,13]
39	40	105.6	157	3092	[16,13,17]
40	41	105.6	157	3289	[13,12,15]
41	42	105.6	157	3464	[16,14,14]
42	43	105.6	157	3143	[14,11,13]
43	44	105.6	157	3397	[16,17,16]
44	45	105.6	157	3193	[16,11,17]
45	46	105.6	157	3472	[15,11,12]
13	47	105.6	157	3423	[16,12,11]
47	48	105.6	157	3339	[119,122,119]
48	49	105.6	157	2902	[122,118,119]
49	50	105.6	157	2893	[122,122,120]
50	51	105.6	157	3318	[117,122,123]
16	52	105.6	157	3400	[39,42,40]
52	53	105.6	157	3312	[40,43,41]
53	54	105.6	157	3230	[43,43,43]
54	55	105.6	157	2937	[41,38,38]
55	56	105.6	157	3061	[38,42,43]
56	57	105.6	157	3487	[42,38,41]
20	58	105.6	157	2823	[50,49,52]
58	59	105.6	157	3247	[48,50,50]
59	60	105.6	157	3004	[49,51,50]
60	61	105.6	157	3485	[47,49,50]
61	62	105.6	157	3178	[52,49,53]
21	63	105.6	157	2856	[13,14,15]
63	64	105.6	157	3367	[12,11,14]
64	65	105.6	157	3011	[13,13,15]
65	66	105.6	157	3078	[13,16,11]
66	67	105.6	157	3260	[11,15,11]
67	68	105.6	157	2942	[16,11,14]
68	69	105.6	157	3406	[15,15,16]
69	70	105.6	157	3359	[15,15,13]

The following subsections examine the actual operating conditions of the system (Section 4.2.1), whereas Section 4.2.2 presents a comparison between EES and other optimization techniques for the optimal placement and sizing of RPCDs.

4.2.1. Assessment of the Preliminary Conditions of the 70-Bus System

To evaluate the benefits associated with the implementation of RPCDs, this subsection examines the system under its actual operating conditions without any reactive power compensation in service. In addition, the system is assumed to operate under the most demanding loading conditions, corresponding to the maximum load values reported in Table 11, with no contribution from the distributed generation connected at bus 52. Accordingly, Table 12 reports the resulting phase voltages and currents. On the one hand, the voltage magnitudes vary from 0.9114 p.u. to 0.993 p.u., with the minimum value falling significantly below the desired operating range of 0.95 p.u. On the other hand, the maximum current is 0.0198 p.u., which remains below the corresponding conductor ampacity and therefore does not represent an operational constraint.

Table 12. Voltage and current magnitudes per bus and phase under actual conditions for the 70-bus system.

Bus or Branch	Voltage Phase a (p.u.)	Voltage Phase b (p.u.)	Voltage Phase c (p.u.)	Current Phase a (p.u.)	Current Phase b (p.u.)	Current Phase c (p.u.)	Ampacity (p.u.)
1	0.9929	0.9929	0.9930	0.0018	0.0019	0.0012	0.7315
2	0.9863	0.9865	0.9864	0.0015	0.0015	0.0011	0.7315
3	0.9802	0.9804	0.9802	0.0014	0.0014	0.0020	0.7315
4	0.9743	0.9745	0.9743	0.0012	0.0015	0.0014	0.7315
5	0.9687	0.9689	0.9687	0.0012	0.0020	0.0012	0.7315
6	0.9638	0.9642	0.9639	0.0017	0.0011	0.0017	0.7315
7	0.9591	0.9595	0.9591	0.0019	0.0012	0.0014	0.7315
8	0.9541	0.9544	0.9540	0.0011	0.0012	0.0014	0.7315
9	0.9498	0.9502	0.9498	0.0017	0.0016	0.0020	0.7315
10	0.9452	0.9454	0.9450	0.0020	0.0017	0.0020	0.7315
11	0.9403	0.9404	0.9401	0.0017	0.0014	0.0013	0.7315
12	0.9354	0.9353	0.9351	0.0013	0.0016	0.0017	0.7315
13	0.9305	0.9303	0.9302	0.0018	0.0019	0.0018	0.7315
14	0.9278	0.9276	0.9275	0.0021	0.0021	0.0021	0.7315
15	0.9252	0.9249	0.9248	0.0011	0.0016	0.0021	0.7315
16	0.9226	0.9222	0.9221	0.0016	0.0016	0.0016	0.7315
17	0.9211	0.9207	0.9207	0.0018	0.0019	0.0016	0.7315
18	0.9195	0.9189	0.9190	0.0011	0.0018	0.0011	0.7315
19	0.9177	0.9172	0.9173	0.0018	0.0021	0.0021	0.7315
20	0.9163	0.9158	0.9159	0.0015	0.0021	0.0016	0.7315
21	0.9157	0.9151	0.9153	0.0019	0.0021	0.0015	0.7315
22	0.9155	0.9149	0.9152	0.0018	0.0015	0.0013	0.7315
23	0.9153	0.9148	0.9151	0.0015	0.0015	0.0013	0.7315
24	0.9152	0.9147	0.9150	0.0019	0.0013	0.0015	0.7315
25	0.9151	0.9146	0.9149	0.0021	0.0018	0.0015	0.7315
26	0.9151	0.9146	0.9149	0.0013	0.0013	0.0011	0.7315
27	0.9914	0.9916	0.9916	0.0055	0.0048	0.0048	0.4521
28	0.9902	0.9905	0.9906	0.0052	0.0048	0.0048	0.4521
29	0.9893	0.9896	0.9898	0.0055	0.0051	0.0052	0.4521
30	0.9886	0.9889	0.9891	0.0055	0.0055	0.0049	0.4521
31	0.9881	0.9884	0.9886	0.0051	0.0052	0.0046	0.4521
32	0.9877	0.9880	0.9882	0.0052	0.0048	0.0048	0.4521
33	0.9875	0.9879	0.9880	0.0051	0.0048	0.0055	0.4521
34	0.9671	0.9674	0.9671	0.0072	0.0073	0.0077	0.4521
35	0.9660	0.9663	0.9660	0.0077	0.0077	0.0075	0.4521

Table 12. *Cont.*

Bus or Branch	Voltage Phase a (p.u.)	Voltage Phase b (p.u.)	Voltage Phase c (p.u.)	Current Phase a (p.u.)	Current Phase b (p.u.)	Current Phase c (p.u.)	Ampacity (p.u.)
36	0.9650	0.9654	0.9651	0.0074	0.0077	0.0077	0.4521
37	0.9644	0.9649	0.9645	0.0080	0.0072	0.0075	0.4521
38	0.9641	0.9646	0.9642	0.0078	0.0077	0.0080	0.4521
39	0.9533	0.9539	0.9534	0.0017	0.0022	0.0020	0.4521
40	0.9527	0.9534	0.9528	0.0025	0.0020	0.0026	0.4521
41	0.9521	0.9530	0.9523	0.0020	0.0019	0.0023	0.4521
42	0.9516	0.9526	0.9518	0.0025	0.0022	0.0022	0.4521
43	0.9512	0.9523	0.9515	0.0022	0.0017	0.0020	0.4521
44	0.9509	0.9521	0.9513	0.0025	0.0026	0.0025	0.4521
45	0.9507	0.9520	0.9511	0.0025	0.0017	0.0026	0.4521
46	0.9506	0.9519	0.9510	0.0023	0.0017	0.0019	0.4521
47	0.9273	0.9272	0.9270	0.0026	0.0019	0.0018	0.4521
48	0.9243	0.9241	0.9240	0.0191	0.0195	0.0191	0.4521
49	0.9224	0.9222	0.9221	0.0196	0.0189	0.0191	0.4521
50	0.9211	0.9209	0.9207	0.0196	0.0196	0.0193	0.4521
51	0.9204	0.9201	0.9200	0.0188	0.0196	0.0198	0.4521
52	0.9211	0.9207	0.9206	0.0063	0.0068	0.0064	0.4521
53	0.9198	0.9194	0.9193	0.0064	0.0069	0.0066	0.4521
54	0.9188	0.9184	0.9183	0.0069	0.0069	0.0069	0.4521
55	0.9181	0.9178	0.9176	0.0066	0.0061	0.0061	0.4521
56	0.9177	0.9173	0.9171	0.0061	0.0068	0.0069	0.4521
57	0.9174	0.9171	0.9169	0.0068	0.0061	0.0066	0.4521
58	0.9150	0.9145	0.9145	0.0081	0.0079	0.0084	0.4521
59	0.9138	0.9133	0.9133	0.0078	0.0081	0.0081	0.4521
60	0.9130	0.9124	0.9124	0.0079	0.0083	0.0081	0.4521
61	0.9123	0.9118	0.9117	0.0076	0.0080	0.0081	0.4521
62	0.9120	0.9115	0.9114	0.0084	0.0080	0.0086	0.4521
63	0.9151	0.9145	0.9147	0.0021	0.0023	0.0024	0.4521
64	0.9145	0.9139	0.9141	0.0019	0.0018	0.0023	0.4521
65	0.9140	0.9134	0.9137	0.0021	0.0021	0.0024	0.4521
66	0.9136	0.9130	0.9133	0.0021	0.0026	0.0018	0.4521
67	0.9133	0.9127	0.9130	0.0018	0.0024	0.0018	0.4521
68	0.9130	0.9124	0.9127	0.0026	0.0018	0.0023	0.4521
69	0.9128	0.9122	0.9126	0.0024	0.0024	0.0026	0.4521
70	0.9127	0.9121	0.9125	0.0024	0.0024	0.0021	0.4521

4.2.2. Determination of the Optimal Placement of Reactive Power Compensation Devices in the 70-Bus System

In this case, the sizing and placement problems were solved using PSO [28], SCA [29], and the whale optimization algorithm (WOA) [30], in addition to GA. However, the optimization study was performed from a single random starting condition, which implies that the optimality of each solution cannot be guaranteed. Regarding the population size and the maximum number of iterations, they remained the same as in the previous case study.

Figure 11 shows the evolution of the optimization process, in which EES did not reach the best solution. Table 13 reports the objective function values and the associated ranking of the solutions after the 100 iterations shown in Figure 11. According to these results, PSO reached the best solution, while EES identified the third-best solution, with a difference of 11.9%. Tables 14–18 present the detailed solutions for each technique. It can be observed that the best solution found (PSO) recommends the adoption of RPCDs at only two buses,

whereas the solution with the highest objective function value (GA) recommends installing RPCDs at many buses across the system. With respect to EES, the configuration suggested lies between these two cases.

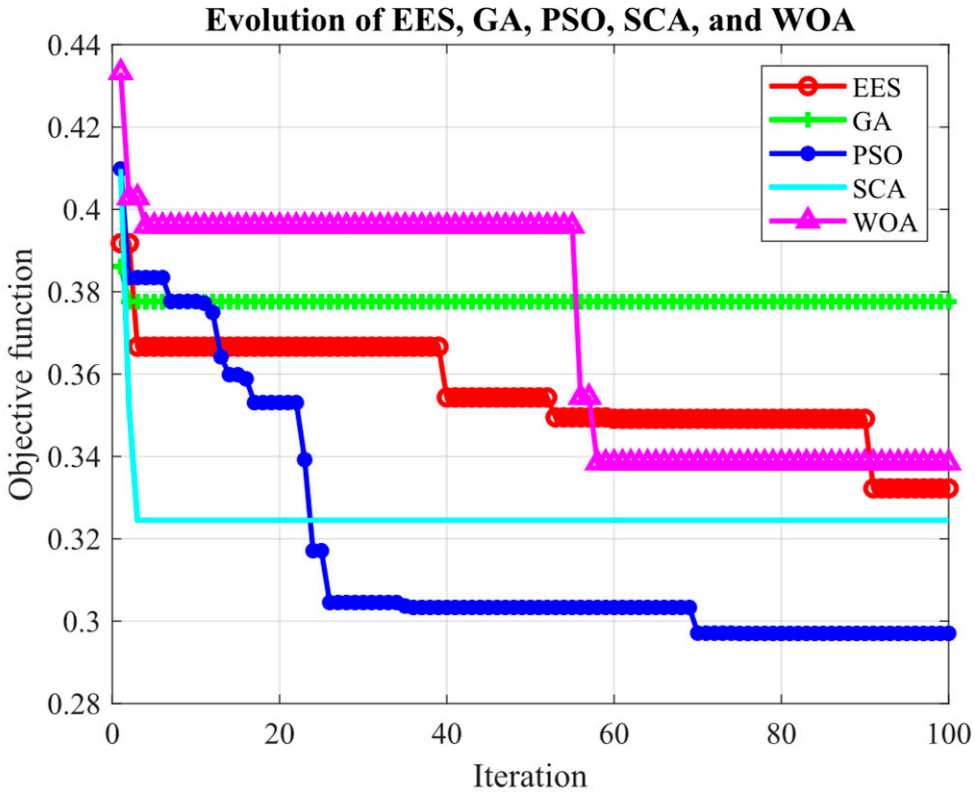

Figure 11. Evolution of the optimization process using several techniques for the 70-bus system.

Table 13. Results of the optimal RPCD placement using several methods for the 70-bus system.

Ranking	Method	Objective Function	Difference Respect to PSO (%)
1	PSO	0.2970	0
2	SCA	0.3245	9.3
3	EES	0.3322	11.9
4	WOA	0.3384	13.9
5	GA	0.3776	27.1

Table 14. Results of the optimal RPCD placement using the PSO for the 70-bus system.

Bus	Reactive Power Phase a (kVAr)	Reactive Power Phase b (kVAr)	Reactive Power Phase c (kVAr)
12	422.1	422.1	415.4
61	419.3	410.6	439.4

Table 15. Results of the optimal RPCD placement using the SCA for the 70-bus system.

Bus	Reactive Power Phase a (kVAr)	Reactive Power Phase b (kVAr)	Reactive Power Phase c (kVAr)
16	459.3	459.3	425.5
70	339.0	363.9	386.6

Table 16. Results of the optimal RPCD placement using the EES for the 70-bus system.

Bus	Reactive Power Phase a (kVAr)	Reactive Power Phase b (kVAr)	Reactive Power Phase c (kVAr)
8	60.2	0	16.7
10	59.6	56.0	3.7
12	38.5	58.6	6.6
13	67.2	115.0	78.7
14	31.8	46.9	88.2
17	0	45.2	0
18	19.2	57.0	52.9
19	0	45.7	0
20	17.3	6.5	151.1
23	7.6	0	0
25	0	6.1	46.8
26	75.8	44.6	18.6
43	0	3.2	35.4
48	18.0	0	8.9
54	3.9	80.3	10.6
55	27.4	55.5	53.4
57	34.0	0	0
58	86.2	51.9	1.6
59	33.7	1.8	26.3
61	45.2	78.4	22.5
62	0	0	24.5
64	26.1	0	95.9
66	44.8	0	6.1
68	0	0	41.6
69	6.7	0	4.6
70	130.4	81.4	29.1

Table 17. Results of the optimal RPCD placement using the WOA for the 70-bus system.

Bus	Reactive Power Phase a (kVAr)	Reactive Power Phase b (kVAr)	Reactive Power Phase c (kVAr)
11	48.9	145.9	65.9
14	71.7	81.5	110.3
18	62.7	46.3	80.1
19	106.3	64.6	116.6
25	38.6	56.5	120.9
29	6.8	21.6	30.7
47	114.9	105.6	43.4
49	85.3	155.7	91.4
60	65.4	112.5	35.3
62	110.4	45.7	62.2
67	115.8	40.5	78.2

Table 18. Results of the optimal RPCD placement using the GA for the 70-bus system.

Bus	Reactive Power Phase a (kVAr)	Reactive Power Phase b (kVAr)	Reactive Power Phase c (kVAr)
4	23.1	47.9	31.4
5	37.1	59.1	8.6
7	0	64.7	0
9	2.9	0	27.2

Table 18. *Cont.*

Bus	Reactive Power Phase a (kVAr)	Reactive Power Phase b (kVAr)	Reactive Power Phase c (kVAr)
11	25.4	0	21.4
13	0	0	29.5
16	18.9	27.2	12.0
18	19.9	49.0	42.2
22	13.9	22.9	22.2
23	35.0	0	66.1
25	34.0	17.7	48.8
31	31.5	21.3	16.1
36	29.9	0	0
37	61.5	0	21.6
39	3.0	33.8	0
40	23.6	19.5	0
42	34.0	0	29.3
43	11.0	50.6	0
45	24.6	9.2	47.9
46	14.2	0	0
48	6.9	30.1	51.7
49	24.9	35.9	18.8
50	21.8	44.5	0
55	60.4	19.5	33.5
56	26.6	34.6	0
57	42.3	31.9	33.2
58	50.4	44.4	54.5
59	38.2	36.1	40.2
60	36.3	49.3	45.5
62	33.6	0	21.1
63	50.2	0	23.1
64	18.3	12.9	17.6
65	32.4	62.5	0
66	1.6	43.2	54.4
67	0	0	29.0
68	56.2	18.3	12.2
69	0	42.7	27.5
70	17.2	18.8	37.0

As EES is the technique under analysis in this paper, Table 19 and Figure 12 present detailed information about the performance of this solution in terms of phase voltages and currents, which are within feasible limits.

Table 19. Voltage and current magnitudes per bus and phase using EES for the 70-bus system.

Bus or Branch	Voltage Phase a (p.u.)	Voltage Phase b (p.u.)	Voltage Phase c (p.u.)	Current Phase a (p.u.)	Current Phase b (p.u.)	Current Phase c (p.u.)	Ampacity (p.u.)
1	0.9952	0.9953	0.9953	0.0018	0.0019	0.0012	0.7315
2	0.9912	0.9913	0.9912	0.0015	0.0015	0.0010	0.7315
3	0.9874	0.9876	0.9873	0.0014	0.0013	0.0020	0.7315
4	0.9838	0.9840	0.9836	0.0012	0.0015	0.0014	0.7315
5	0.9804	0.9807	0.9802	0.0012	0.0020	0.0012	0.7315
6	0.9778	0.9782	0.9775	0.0017	0.0011	0.0017	0.7315

Table 19. *Cont.*

Bus or Branch	Voltage Phase a (p.u.)	Voltage Phase b (p.u.)	Voltage Phase c (p.u.)	Current Phase a (p.u.)	Current Phase b (p.u.)	Current Phase c (p.u.)	Ampacity (p.u.)
7	0.9753	0.9757	0.9750	0.0018	0.0012	0.0014	0.7315
8	0.9726	0.9731	0.9722	0.0078	0.0012	0.0021	0.7315
9	0.9704	0.9711	0.9699	0.0017	0.0015	0.0020	0.7315
10	0.9680	0.9689	0.9674	0.0076	0.0071	0.0018	0.7315
11	0.9653	0.9664	0.9649	0.0017	0.0014	0.0012	0.7315
12	0.9626	0.9640	0.9624	0.0049	0.0076	0.0015	0.7315
13	0.9598	0.9614	0.9601	0.0087	0.0152	0.0103	0.7315
14	0.9587	0.9604	0.9595	0.0040	0.0059	0.0115	0.7315
15	0.9577	0.9594	0.9586	0.0011	0.0015	0.0020	0.7315
16	0.9568	0.9583	0.9578	0.0015	0.0015	0.0015	0.7315
17	0.9566	0.9578	0.9578	0.0017	0.0057	0.0015	0.7315
18	0.9564	0.9570	0.9579	0.0024	0.0074	0.0070	0.7315
19	0.9562	0.9560	0.9579	0.0017	0.0058	0.0020	0.7315
20	0.9561	0.9550	0.9580	0.0022	0.0018	0.0204	0.7315
21	0.9565	0.9545	0.9583	0.0019	0.0020	0.0014	0.7315
22	0.9566	0.9544	0.9583	0.0017	0.0014	0.0012	0.7315
23	0.9567	0.9543	0.9584	0.0013	0.0014	0.0012	0.7315
24	0.9568	0.9543	0.9586	0.0019	0.0012	0.0014	0.7315
25	0.9569	0.9544	0.9587	0.0020	0.0015	0.0060	0.7315
26	0.9572	0.9544	0.9587	0.0101	0.0058	0.0023	0.7315
27	0.9937	0.9939	0.9940	0.0055	0.0048	0.0048	0.4521
28	0.9926	0.9929	0.9929	0.0052	0.0048	0.0048	0.4521
29	0.9917	0.9920	0.9921	0.0055	0.0051	0.0052	0.4521
30	0.9910	0.9913	0.9914	0.0055	0.0055	0.0049	0.4521
31	0.9904	0.9908	0.9909	0.0051	0.0052	0.0046	0.4521
32	0.9900	0.9904	0.9905	0.0052	0.0048	0.0048	0.4521
33	0.9898	0.9903	0.9903	0.0051	0.0048	0.0055	0.4521
34	0.9789	0.9792	0.9786	0.0071	0.0073	0.0076	0.4521
35	0.9777	0.9781	0.9775	0.0076	0.0076	0.0074	0.4521
36	0.9768	0.9772	0.9766	0.0073	0.0076	0.0076	0.4521
37	0.9762	0.9767	0.9760	0.0079	0.0071	0.0074	0.4521
38	0.9759	0.9764	0.9757	0.0077	0.0076	0.0079	0.4521
39	0.9719	0.9725	0.9717	0.0017	0.0021	0.0020	0.4521
40	0.9712	0.9720	0.9713	0.0024	0.0020	0.0026	0.4521
41	0.9706	0.9716	0.9710	0.0020	0.0018	0.0023	0.4521
42	0.9700	0.9712	0.9708	0.0024	0.0021	0.0021	0.4521
43	0.9696	0.9710	0.9706	0.0021	0.0015	0.0044	0.4521
44	0.9693	0.9708	0.9704	0.0024	0.0026	0.0024	0.4521
45	0.9691	0.9707	0.9702	0.0024	0.0017	0.0026	0.4521
46	0.9690	0.9706	0.9701	0.0023	0.0017	0.0018	0.4521
47	0.9568	0.9583	0.9571	0.0025	0.0019	0.0017	0.4521
48	0.9540	0.9553	0.9542	0.0175	0.0189	0.0180	0.4521
49	0.9521	0.9534	0.9523	0.0190	0.0183	0.0185	0.4521
50	0.9508	0.9521	0.9510	0.0190	0.0190	0.0187	0.4521
51	0.9501	0.9514	0.9503	0.0182	0.0190	0.0192	0.4521
52	0.9555	0.9574	0.9563	0.0060	0.0065	0.0062	0.4521
53	0.9544	0.9568	0.9551	0.0062	0.0067	0.0064	0.4521
54	0.9536	0.9564	0.9542	0.0065	0.0102	0.0062	0.4521
55	0.9532	0.9559	0.9537	0.0058	0.0074	0.0072	0.4521
56	0.9529	0.9554	0.9533	0.0059	0.0065	0.0067	0.4521
57	0.9528	0.9551	0.9530	0.0062	0.0059	0.0064	0.4521
58	0.9555	0.9540	0.9567	0.0111	0.0079	0.0080	0.4521

Table 19. *Cont.*

Bus or Branch	Voltage Phase a (p.u.)	Voltage Phase b (p.u.)	Voltage Phase c (p.u.)	Current Phase a (p.u.)	Current Phase b (p.u.)	Current Phase c (p.u.)	Ampacity (p.u.)
59	0.9546	0.9531	0.9557	0.0069	0.0077	0.0070	0.4521
60	0.9539	0.9526	0.9550	0.0076	0.0079	0.0078	0.4521
61	0.9534	0.9523	0.9544	0.0073	0.0103	0.0070	0.4521
62	0.9530	0.9521	0.9542	0.0081	0.0076	0.0074	0.4521
63	0.9566	0.9539	0.9583	0.0020	0.0022	0.0023	0.4521
64	0.9567	0.9533	0.9585	0.0033	0.0017	0.0126	0.4521
65	0.9570	0.9529	0.9582	0.0020	0.0020	0.0023	0.4521
66	0.9573	0.9525	0.9581	0.0057	0.0025	0.0015	0.4521
67	0.9575	0.9523	0.9580	0.0017	0.0023	0.0017	0.4521
68	0.9578	0.9523	0.9580	0.0025	0.0017	0.0052	0.4521
69	0.9582	0.9522	0.9578	0.0021	0.0023	0.0023	0.4521
70	0.9588	0.9523	0.9577	0.0173	0.0106	0.0036	0.4521

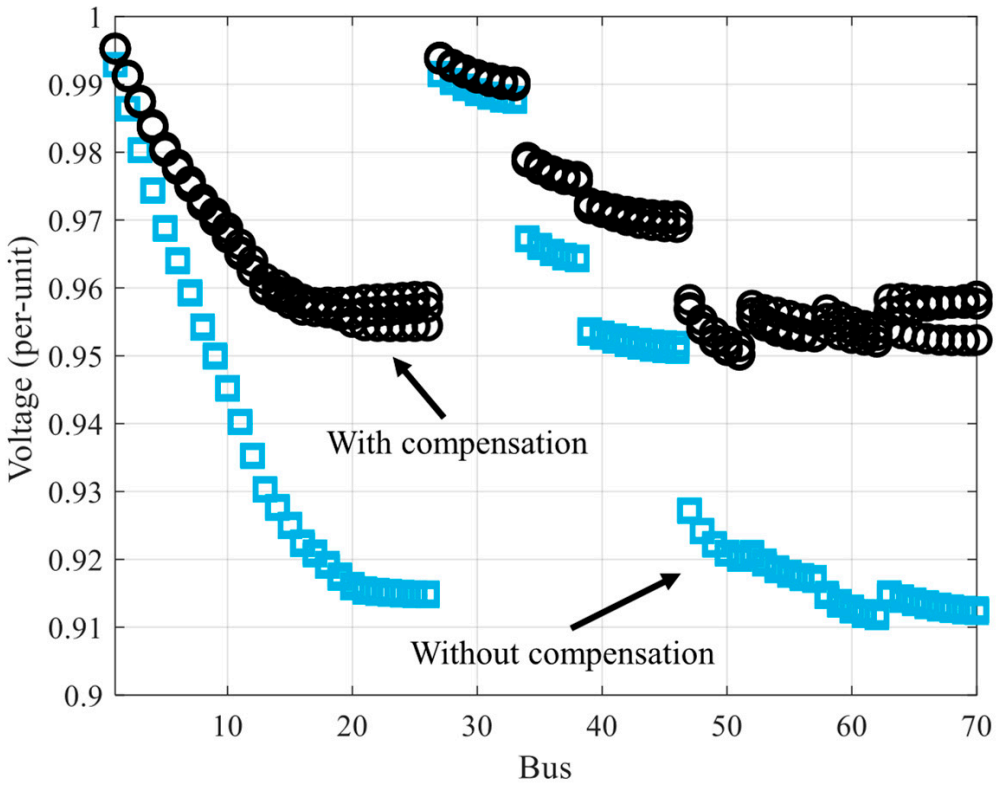

Figure 12. Voltage profile of the 70-bus system.

5. Discussion and Conclusions

This paper presented a comprehensive methodology for the optimal sizing and placement of RPCDs in DSs, a problem characterized by the simultaneous consideration of multiple techno-economic factors and strong interdependencies between decision variables. Owing to its computational complexity, this problem is well-suited to heuristic optimization approaches.

Unlike most existing studies, which typically rely on the simplifying assumption of balanced network operation, the proposed framework is designed to better reflect the actual operating conditions of DSs. In this context, the EES was applied to the RPCD design problem. To the best of the authors' knowledge, this work represents the first application

of EES in this domain, demonstrating its suitability as a computationally efficient tool for obtaining high-quality techno-economic solutions.

The optimal sizing and placement of RPCDs were formulated as two distinct yet interdependent optimization problems and addressed in an integrated manner. The placement problem was modeled using binary encoding, while the reactive power dispatch problem was formulated using real-valued encoding. This coordinated approach enabled the effective interaction between both problems, ensuring feasibility while maintaining solution quality.

Simulation results obtained from the analysis of two rural DSs confirm the effectiveness of the proposed methodology. The first case study consisted of a system with 15 buses, while the second involved a system with 70 buses.

In the first case (15-bus system), the objective function was explored extensively by repeatedly performing the optimization process using EES and GA. This approach allows the identification of a solution with a high probability of being the global optimum. Although this methodology requires substantial computational resources, it helps overcome the main limitation of heuristic approaches, which is related to the degree of optimality of the obtained solution. According to the results, EES outperformed GA by 7.4%.

In the second case (70-bus system), only a single random starting condition was considered; however, a larger number of techniques, including GA, PSO, SCA, and WOA, were incorporated into the comparative analysis. According to the observed results, EES ranked in the middle, with a difference of 11.9% compared with the solution recommended by PSO.

Overall, the results confirm that the proposed EES-based framework constitutes a reliable and efficient approach for the coordinated sizing and placement of RPCDs in DSs. However, some aspects have not been included in the present formulation, or have been included but not investigated in depth:

First, the parameter c of EES employed in Equations (24)–(29) was arbitrarily defined to follow a linear behavior with the iterations of the optimization process. Other functions have been proposed in the literature—for example, exponential functions—that have not been tested here and could improve the performance of EES.

Second, the unbalanced nature of DSs was incorporated into the selection and placement of RPCDs. However, no specific measure was included to mitigate such unbalance. In other words, a method was developed to force the voltage magnitude within the interval [0.95 p.u., 1.05 p.u.]; however, within this interval, the phase voltages may still differ significantly.

Third, this method was implemented considering only the most severe operating condition, in which the load demand is maximal and the contribution of distributed generation is negligible. However, this is not always the case from an operational perspective; therefore, a probabilistic formulation could be beneficial.

These three aspects are expected to be addressed in future work.

Author Contributions: J.M.L.-R. contributed in the areas of funding acquisition, conceptualization, software development, writing—original draft preparation, and formal analysis. R.D.-L. contributed in the areas of funding acquisition, methodology, resources, formal analysis, and software development. J.S.A.-S. contributed in the areas of funding acquisition, data curation, visualization, investigation, and resources. J.L.B.-A. contributed in the areas of funding acquisition, project administration, investigation, validation, and supervision. All authors have read and agreed to the published version of the manuscript.

Funding: This work was supported by the Spanish Government (Ministerio de Ciencia, Innovación y Universidades—Proyectos de Generación de Conocimento 2024) under Grant PID2024-160489OB-I00.

Institutional Review Board Statement: Not applicable.

Informed Consent Statement: Not applicable.

Data Availability Statement: The original contributions presented in this study are included in the article. Further inquiries can be directed to the corresponding author.

Acknowledgments: During the preparation of this work, the authors used ChatGPT-5 in order to improve the language and readability of the manuscript. After using this service, the authors reviewed and edited the content as needed and take full responsibility for the content of the publication.

Conflicts of Interest: The authors declare no conflicts of interest.

References

1. Ismail, B.; Wahab, N.I.A.; Othman, M.L.; Radzi, M.A.M.; Vijyakumar, K.N.; Naain, M.N.M. A comprehensive review on optimal location and sizing of reactive power compensation using hybrid-based approaches for power loss reduction, voltage stability improvement, voltage profile enhancement and loadability enhancement. *IEEE Access* **2020**, *8*, 222733–222765. [CrossRef]
2. Majidzadeh, M.; Esmaeeli, M.; Afkar, H.; Golshannavaz, S.; Li, Z. Optimal reactive power planning in an industrial microgrid: A case study of Urmia Petrochemical Plant. *Glob. Energy Interconnect.* **2025**, *9*, 208–218. [CrossRef]
3. Asabere, P.; Sekyere, F.; Ayambire, P.; Ofosu, W.K. Optimal capacitor bank placement and sizing using particle swarm optimization for power loss minimization in distribution network. *J. Eng. Res.* **2025**, *13*, 1307–1315. [CrossRef]
4. Rajak, S.; Saha, M.; Das, B.; Chaduvula, H. Optimum enhancement of voltage profile of the droop controlled islanded microgrid by incorporating shunt capacitors and active power DGs using PSO and SPBO algorithm. *Next Energy* **2025**, *9*, 100470. [CrossRef]
5. Adegoke, S.A. Optimal sizing and placement of capacitors using an improved particle swarm optimization to enhance networks reliability and voltage profile distribution systems. *Energy Convers. Manag.—X* **2025**, *28*, 101294. [CrossRef]
6. Amekah, E.D.; Ramde, E.W.; Quansah, D.A.; Twumasi, E.; Meilinger, S.; Schneiders, T. Evaluating the effect of reactive power injection on power factor and system losses reduction in an optimally sized PV grid-connected solar photovoltaic system. *Sol. Compass* **2026**, *17*, 100149. [CrossRef]
7. Jahed, Y.G.; Mousavi, S.Y.M.; Golestan, S. Optimal sizing and siting of distributed generation systems incorporating reactive power tariffs via water flow optimization. *Electr. Power Syst. Res.* **2024**, *231*, 110278. [CrossRef]
8. Bhattacharyya, B.; Rajbhar, S.K.; Basak, S. Optimal co-ordination of multitype FACTS controllers for reactive power optimization. *Electr. Power Syst. Res.* **2026**, *253*, 112520. [CrossRef]
9. Bhattacharyya, B.; Rajbhar, S.K. Optimal VAr management of a large power network using most efficient method of weak node detection. *Meas. Energy* **2025**, *8*, 100077. [CrossRef]
10. Gómez, J.; De Marco, F.; Reigosa, D. Optimal sizing and placement of synchronous condensers with adaptive search-space reduction. *Electr. Power Syst. Res.* **2026**, *254*, 112607. [CrossRef]
11. Singh, A.K.; Kumar, A. Optimal deployment of reactive power in a renewable energy sources integrated system with EVs demand using local randomized neural networks. *Renew. Energy Focus* **2025**, *54*, 100719. [CrossRef]
12. Ebeed, M.; Ali, S.; Kassem, A.M.; Hashem, M.; Kamel, S.; Hussien, A.G.; Jurado, F.; Mohamed, E.A. Solving stochastic optimal reactive power dispatch using an adaptive beluga whale optimization considering uncertainties of renewable energy resources and the load growth. *Ain Shams Eng. J.* **2024**, *15*, 102762. [CrossRef]
13. Alnami, H. Reactive power control of distribution networks based on optimal capacitor allocation. *J. Eng. Res.* 2025, *in press*. [CrossRef]
14. Mathenge, S.W.; Mharakurwa, E.T.; Mogaka, L. Voltage enhancement and loss minimization in a radial network through optimal capacitor sizing and placement based on crow search algorithm. *Energy Rep.* **2024**, *12*, 4953–4965. [CrossRef]
15. Sharma, S.; Ghosh, S. Optimal planning and placement of capacitor in distribution system based on particle swarm and hybrid bee-cuckoo search under varying load conditions. *Energy Rep.* **2025**, *13*, 5219–5237. [CrossRef]
16. Badrudeen, T.U.; Ariyo, F.K.; Nwulu, N. Optimal sizing of FACTS controller through hybrid metaheuristic algorithm for static security enhancement in transmission power systems. *Sci. Afr.* **2025**, *27*, e02543. [CrossRef]
17. Patiño, J.E.S.; Pareja, L.A.G.; Carmona, O.G. Optimal placement, sizing and operation of D-STATCOMs in power distribution systems using a mixed-integer linear programming model. *Results Eng.* **2025**, *26*, 104749. [CrossRef]
18. Patel, K.P.; Patel, N.A.; Chaudhari, J.P.; Mewada, H.K. Optimal placement of DSTATCOMs and PID tuned controller in IEEE bus system for enhanced voltage stability and power loss reduction under RES integration using hybrid BWO-SSA algorithm. *Results Eng.* **2025**, *28*, 108216. [CrossRef]
19. Okendo, E.O.; Farzaneh, H. Multi-objective optimal sizing and location of the grid-connected renewable microgrids, considering cost-effectiveness, power loss, and network stability approaches. *Energy Convers. Manag.—X* **2026**, *29*, 101465. [CrossRef]

20. Das, T.; Roy, R.; Mandal, K.K. Solving hybrid high voltage AC-DC optimal reactive power dispatch problem using JAYA algorithm. *Meas. Digit.* **2025**, *4*, 100017. [CrossRef]
21. Fotis, G. An improved arithmetic method for determining the optimum placement and size of EV charging stations. *Comput. Electr. Eng.* **2024**, *120*, 109840. [CrossRef]
22. Short, T.A. *Electric Power Distribution Handbook*; CRC Press LLC: Boca Raton, FL, USA, 2004.
23. Teng, J.H. A direct approach for distribution system load flow solutions. *IEEE Trans. Power Deliv.* **2003**, *18*, 882–887. [CrossRef]
24. Jia, H.; Rao, H. Experience exchange strategy: An evolutionary strategy for meta-heuristic optimization algorithms. *Swarm Evol. Comput.* **2025**, *98*, 102082. [CrossRef]
25. Chuang, Y.C.; Chen, C.T.; Hwang, C. A real-coded genetic algorithm with a direction-based crossover operator. *Inf. Sci.* **2015**, *305*, 320–348. [CrossRef]
26. Chuang, Y.C.; Chen, C.T.; Hwang, C. A simple and efficient real-coded genetic algorithm for constrained optimization. *Appl. Soft Comput.* **2016**, *38*, 87–105. [CrossRef]
27. Finch, S.J.; Mendell, N.R.; Thode, H.C.J. Probabilistic measures of adequacy of a numerical search for a global maximum. *J. Am. Stat. Assoc.* **1989**, *84*, 1020–1023. [CrossRef]
28. Beheshti, Z. A time-varying mirrored S-shaped transfer function for binary particle swarm optimization. *Inf. Sci.* **2020**, *512*, 1503–1542. [CrossRef]
29. Mirjalili, S. SCA: A Sine Cosine Algorithm for solving optimization problems. *Knowl.-Based Syst.* **2016**, *96*, 120–133. [CrossRef]
30. Mirjalili, S. The whale optimization algorithm. *Adv. Eng. Softw.* **2016**, *95*, 51–67. [CrossRef]